

Cascade and Damping of Alfvén-Cyclotron Fluctuations: Application to Solar Wind Turbulence

Yan Wei Jiang,^{1,2} Siming Liu,³ and Vahé Petrosian,^{1,2,4}

ABSTRACT

It is well-recognized that the presence of magnetic fields will lead to anisotropic energy cascade and dissipation of astrophysical turbulence. With the diffusion approximation and linear dissipation rates, we study the cascade and damping of Alfvén-cyclotron fluctuations in solar plasmas numerically for two diagonal diffusion tensors, one (isotropic) with identical components for the parallel and perpendicular directions (with respect to the magnetic field) and one with different components (non-isotropic). It is found that for the isotropic case the steady-state turbulence spectra are nearly isotropic in the inertial range and can be fitted by a single power-law function with a spectral index of $-3/2$, similar to the Iroshnikov-Kraichnan phenomenology, while for the non-isotropic case the spectra vary greatly with the direction of propagation. The energy fluxes in both cases are much higher in the perpendicular direction than in the parallel direction due to the angular dependence (or inhomogeneity) of the components. In addition, beyond the MHD regime the kinetic effects make the spectrum softer at higher wavenumbers. In the dissipation range the turbulence spectrum cuts off at the wavenumber, where the damping rate becomes comparable to the cascade rate, and the cutoff wavenumber changes with the wave propagation direction. The angle averaged turbulence spectrum of the isotropic model resembles a broken power-law, which cuts off at the maximum of the cutoff wavenumbers or the ^4He cyclotron frequency. Taking into account the Doppler effects, the model naturally reproduces the broken power-law turbulence spectra observed in the solar wind and predicts that a higher break frequency always comes along with a softer dissipation range spectrum that may be caused by the increase of the

¹Center for Space Science and Astrophysics, Department of Physics, Stanford University, Stanford, CA 94305; arjiang@stanford.edu, vahep@astronomy.edu

²Kavli Institute of Particle Physics and Cosmology, Stanford University

³Department of Physics and Astronomy, University of Glasgow, Glasgow, G12 8QQ, UK; sliu@astro.gla.ac.uk

⁴Also Department of Applied Physics

turbulence intensity, the reciprocal of the plasma β_p , and/or the angle between the solar wind velocity and the mean magnetic field. These predictions can be tested by detailed comparisons with more accurate observations.

Subject headings: MHD — plasmas — solar wind — turbulence — waves

1. Introduction

Turbulence is ubiquitous in the universe and plays important roles in our understanding of many natural phenomena (Kolmogorov 1941; Iroshnikov 1963; Kraichnan 1965). It occurs in highly non-equilibrium systems, where the microscopic viscous and/or resistive dissipation processes cannot effectively convert the free energy into the internal energy of the fluid. Such systems usually have very high Reynolds numbers and/or cover huge spatial and temporal scales, so that the free energy is stored in the large scale motions and/or magnetic fields. For plasmas, the free energy initially may also be stored in non-equilibrium distributions of charged particles. Turbulence is generated through a variety of instabilities related either to the large scale magneto-hydrodynamic (MHD) processes or the microscopic collective plasma effects and/or plasma physics processes (Borovsky & Funsten 2003). These aspects have been extensively investigated with the MHD and/or plasma physics theories. In astrophysics, most turbulence is carried by magnetized plasmas. It is responsible for distributing energies among different components of the plasmas, which may result in distinct emission characteristics or other observable features. Observations of these radiations can be used to study the corresponding astrophysical sources [e.g., Liu et al. (2004, 2006) on ^3He rich impulsive solar energetic particle events].

Plasma waves or turbulence once generated (usually on large scales comparable to the dynamical scales given the large amount of energy inferred from astrophysical observations) undergo two types of interactions: wave-wave and wave-particle. The former dominates at large scales, where the Reynolds (ordinary or magnetic or both) number is large, and results in an almost dissipationless cascade primarily to smaller scales and higher values of the wavenumber k . The interactions of waves with the more numerous low energy particles gradually become more important as the cascade reaches short enough scales (and the Reynolds number approaches unity and/or the kinetic effects set in) and damp the waves. This results in plasma heating and/or particle acceleration. The wave-particle interactions also determine the spatial diffusion and energizing of high energy particles in collisionless turbulent plasmas and are essential elements of the cosmic ray theory (Ginzburg & Syrovatskii 1969; Yan & Lazarian 2002). The spectral range from the turbulence generation scale k_0 to the damping scale k_{max} is called the *inertial range*, where the angle averaged energy flux is inde-

pendent of k . Beyond this range, there are strong couplings between the charged background particles and turbulent motions. For collisional plasmas, where the Coulomb collision mean free path is much shorter than other relevant spatial scales, the energy from the turbulence dissipation is thermalized quickly and the result is plasma heating. Much astrophysical turbulence, however, is carried by collisionless plasmas, where the Coulomb mean free path is long. Although it is generally accepted that the particle distributions in these plasmas are determined by couplings of the (charged) particles with the turbulent electro-magnetic fluctuations, the details of these interactions are not well understood. The wave damping, which usually occurs on the smallest spatial scales, has been an essential part of plasma physics theories for collisionless but presumably *thermal* plasmas [see e.g., Braginskii (1965); André (1985); Gary & Borovsky (2004)]. There is little work on damping by nonthermal particle distributions. Recently, Petrosian et al. (2006) derived the transit-time damping (TTD) rate of fast-mode waves by an arbitrary energy distribution of electrons and protons under typical solar-flare conditions. Large scale waves in this case can be damped by high energy particles through resonant wave-particle couplings. The studies of the turbulent energy dissipation in general and the particle acceleration from a low energy background to high energies in particular require a more complete (beyond the MHD regime) treatment of the wave cascade and damping.

The cascade process has been an essential element in all kinds of turbulence studies. The highly nonlinear nature of turbulence makes this a very challenging aspect of the problem. Nevertheless, the energy transfer of isotropic incompressible hydrodynamical turbulence, the simplest form of turbulence, has been described reasonably well with the Kolmogorov phenomenology that assumes a scale-independent self-similar cascade process, leading to the famous Kolmogorov power-law spectrum with a (one dimensional isotropic) spectral index of $-5/3$ in the inertial range (Kolmogorov 1941). Most astrophysical plasmas carry magnetic fields so that large scale MHD waves and small scale kinetic plasma fluctuations may be excited. The wave propagation effects on the cascade of MHD turbulence were first discussed by Iroshnikov (1963) and Kraichnan (1965). Although MHD effects are expected to introduce anisotropy to the system that can affect the couplings between the turbulence and background particles significantly, these preliminary investigations assumed that the turbulence is isotropic and reduced the cascade to a one-dimensional (1D) problem, yielding a spectral index of $-3/2$ (Zhou & Matthaeus 1990). This is called the Iroshnikov-Kraichnan (IK) phenomenology. Since both the Kolmogorov and IK cascade timescales ($\propto k^{-2/3}$ and $k^{-1/2}$, respectively) decline with increasing k (or decreasing spatial scales) more slowly than the periods of MHD waves ($\propto k^{-1}$), the turbulence may be better described as spectra of waves at higher values of k 's (smaller spatial scales), which play a critical role in the energizing of low energy background particles. However, at such high values of k 's one may

be stepping beyond the MHD regime and must use more complex dispersion relations to take into account the kinetic effects and the anisotropy of the turbulence properly (Leamon et al. 2000; Markovskii et al. 2006).

To study the anisotropic effects induced by the presence of large scale magnetic fields, MHD turbulence has been treated as an ensemble of linear wave modes [e.g., Cho et al. (2003)]. Its nonlinear nature is revealed in the wave-wave couplings. Although this quasi-linear treatment may not be valid for strong turbulence, it is certainly a good approximation when the magnetic field fluctuations are much smaller than the large scale field and the wave periods are much shorter than the eddy turnover timescales (Galtier 2006). Significant insight of properties of Alfvén and magnetosonic turbulence has been obtained recently through this approach (Sridhar & Goldreich 1994; Goldreich & Sridhar 1995; Galtier et al. 2000; Chandran 2005). However, the component of Alfvén turbulence excitations nearly perpendicular to a large scale magnetic field is dominated by nonlinear effects (Montgomery & Turner 1981). This indicates inherent limitations of treating MHD turbulence as a spectrum of waves (Galtier 2006). As shown by Montgomery & Matthaeus (1995), linear MHD wave modes do not give a complete description of turbulence excitations and their couplings, and treating MHD turbulence as an ensemble of linear wave modes may miss some critical nonlinear effects (Ng & Bhattacharjee 1997). This is more evident in hydrodynamic simulations of decaying turbulence, where the compressible wave component accounts for about 10% of the turbulence kinetic energy (Porter et al. 1998, 1999). MHD simulations give similar results (Matthaeus et al. 1996; Vestuto et al. 2003). These studies suggest that treating turbulence as a spectrum of linear wave modes may not describe the dominant energy component properly, which also reflects the highly non-linear nature of a fully developed turbulence, especially on large scales, where the wave periods may be longer than the turbulence cascade timescale (Borovsky & Funsten 2003).

Based on the dominance of nonlinear or wave-propagation effects, Oughton et al. (2006) recently separated the Alfvén turbulence into two interacting parts: quasi-two-dimensional (2D) and wave-like fluctuations. The quasi-2D component characterizes the nearly perpendicular excitations and may be described with a quasi-2D Kolmogorov phenomenology. The wave-like fluctuations may be described with an IK phenomenology with propagation direction dependent wave periods. The cascade of turbulence then also depends on the assumed couplings of these two components. It is interesting to note that the two components are separated by the critical balance between linear wave periods and nonlinear eddy turnover timescales, and the incompressible strong Alfvén turbulence described by Goldreich & Sridhar (1995) appears to be appropriate for the quasi-2D component that is dominated by nonlinear effects. Due to the suppression of cascade by wave propagation effects, Alfvén turbulence with wave periods proportional to the parallel component of

wavevectors cascades preferentially in the direction perpendicular to the mean magnetic field. The wave-like fluctuations need longer time to develop, which may explain the exponential cutoff of the power spectrum in the direction parallel to the mean large scale magnetic field observed in MHD simulations (Cho et al. 2002).

Advances in computational power and numerical algorithms over the past few decades have made numerical simulations one of the important tools for quantitative investigations of magnetized turbulence (Shebalin et al. 1983; Matthaeus et al. 1998; Cho et al. 2002, 2003; Cho & Lazarian 2003). However, turbulence usually covers a huge dynamical range from the macroscopic scales of turbulence generation to the microscopic dissipation scales. Current simulations have a dynamical range of a few hundreds to a few thousands and have not been able to give a complete description of energy flows in magnetized turbulence, limiting their astrophysical applications. Moreover, most of these studies are limited to the MHD regime, where the background particles are strongly coupled with each other and can be treated together as a single fluid. The electron magnetohydrodynamics (EMHD) treats electrons and ions as two fluids. It is only applicable in a narrow frequency range between the electron and ion gyro-frequencies, where the whistler dispersion relation is valid (Biskamp et al. 1999; Petrosian & Liu 2004). Recently Galtier (2006) showed that the transition from the MHD to the EMHD may be studied with the incompressible Hall MHD for weak turbulence. However, a quantitative weak turbulence theory is still to be developed, and it is not obvious how a complete theory may cover both the weak and strong turbulence regimes. To address the heating of background particles by turbulence, one usually assumes that most of the background particles reach thermal distributions and arbitrarily extrapolates the turbulence spectrum into the dissipation range, where the MHD, Hall MHD, and EMHD formalisms may be invalid [e.g., Leamon et al. (1999); Tu et al. (2002); Zhang & Li (2004); Wu & Yang (2006)]. The particle-in-cell and kinetic simulations can usually study processes near the gyro-scales of the background particles (Gary, Saito, & Li 2008; Howes et al. 2008).

Observations of solar corona, solar flares, solar winds, and space plasmas, on the other hand, demand a detailed study of the turbulence evolution over a large dynamical range. There are no direct observations of turbulence in solar corona and solar flares, but the observed high Reynolds numbers and models for particle acceleration demand existence of turbulent plasma waves (Brown & Melrose 1977; Miller & Roberts 1995; Fletcher & Hudson 2008; Krucker et al. 2008b). *In situ* observations of space plasmas reveal evidence of wave-particle interactions (Parks et al. 2006; Chen et al. 2007), turbulence generation and dissipation, and the dominance of the turbulence (in the Earth’s plasma sheet) by eddies instead of plasma waves (Borovsky & Funsten 2003). In solar winds, direct measurements of the turbulence spectrum over more than 6 orders of magnitude in frequency challenge all existing theoretical models (Denskat et al. 1983). Indeed, strong anisotropies are observed

in almost all the relevant spatial scales (Hamilton et al. 2008; Osman & Horbury 2007; Dasso et al. 2005; Matthaeus et al. 1990). While the turbulence anisotropy at large scales, which is likely related to the turbulence generation mechanism, appears to be correlated with the solar wind speed (Dasso et al. 2005), at smaller scales the quasi-2D component always dominates, which should be attributed to the dynamics of the turbulence cascade (Hamilton et al. 2008). At even higher frequencies, there is a spectral break, which has been attributed to the onset of dissipation or kinetic effects by the background particles (Li et al. 2001; Stawicki et al. 2001; Galtier 2006; Howes et al. 2008a). In the dissipation range and kinetic effect dominant regime, background particles with different charge to mass ratios interact with the electromagnetic fluctuations quite differently (Petrosian & Liu 2004; Liu et al. 2004, 2006; Leamon et al. 1998). This results in complicated wave dispersion relations, namely the dependence of the wave frequency on the wavevector (André 1985), and certainly affects the turbulence cascade. The couplings among waves and particles are also complicated (Stix 1962; Xie & Ofman 2004; Saito & Gary 2007). Thus for practical applications one requires a more readily solvable approach and algorithm, which can utilize the basic physics learned from detailed simulations in an approximate but numerically effective manner.

The diffusion approximation for the power spectrum in the wavevector space has been a very efficient tool to study the turbulence cascade and dissipation over a large dynamical range (Zakharov & Kuznetsov 1978). Although the diffusion equation may not be derived from the fluid dynamical equations, especially for weak turbulence (Ng & Bhattacharjee 1997; Galtier et al. 2000), it has several achievements in quantitative studies of the MHD turbulence. The 1D models not only address the transition of turbulence from the large scale Kolmogorov phenomenology to the small scale IK cascade (Zhou & Matthaeus 1990), but also are used to study the acceleration and heating of background particles by magnetized turbulence (Miller & Roberts 1995; Miller et al. 1996) and the damping of waves at small scales (Li et al. 2001). These studies have deepened our understanding of energy release processes during solar flares significantly. However, they encounter difficulties in reproducing the observed broken power-law spectrum of solar wind magnetic fluctuations (Li et al. 2001; Stawicki et al. 2001). Due to the nonlinear nature of these 1D diffusion models, the turbulence spectrum cuts off sharply at the wavenumber, where the cascade timescale becomes comparable to the wave damping time.

Studies of weak Alfvén turbulence with the quasi-linear treatment of electromagnetic fluctuations have shown that the cascade is anisotropic (Galtier 2006). It is also well-known that damping rates of different plasma wave modes by thermal background particles are very sensitive to the wave propagation direction [see e.g., Ginzburg (1961); Gary & Borovsky (2004); Petrosian et al. (2006)]. These anisotropies are critical to study the energy dis-

sipation through magnetized turbulence in a collisionless thermal plasma. Thus, 2D diffusion models are needed to advance our understanding of magnetized turbulence and address the difficulties encountered with the 1D models. Cranmer & van Ballegoijen (2003) have shown recently that the heating of the background particles by Alfvén turbulence are very sensitive to the 2D and kinetic effects. To recover the critical balance proposed by Goldreich & Sridhar (1995) and partially take into account the kinetic effects, they constructed a complicated advection-diffusion equation for the power spectrum with three dimensionless coefficients. A similar quasi-2D model was proposed recently by Howes et al. (2007, 2008a) to explain the broken power-law character of the power spectrum of the turbulent magnetic field fluctuations in the solar wind.

In this paper, we study the general characteristics of the nonlinear 2D diffusion model with the kinetic and damping effects of Alfvén-cyclotron fluctuations treated self-consistently. In principle, all plasma mode branches, such as Alfvén, fast, and slow modes, and their extension beyond the MHD regime at small scales, should be included to have a complete description of the cascade and damping of magnetized turbulence. One then needs to solve a set of coupled diffusion equations for each wave mode branch (André 1985). This is a quite challenging task because the results will depend on both the interactions within each wave mode branch and couplings among different branches. Cho & Lazarian (2003) showed that couplings among different mode branches are usually weak, and Luo & Melrose (2006) showed that these couplings decrease toward small spatial scales. Chandran (2005), on the other hand, found that the couplings between Alfvén and fast modes are significant in the direction parallel to the large scale magnetic field, where the frequencies of the Alfvén and fast modes are comparable. The couplings among different branches therefore can be separated from other processes near the dissipation range, where the kinetic and damping effects dominate.

We use the exact dispersion relation for a cold plasma (to go beyond the MHD regime), which is a good approximation for the more general dispersion relation of a collisionless thermal plasma. The diffusion coefficients are constructed as a function of the wave frequency, phase or group velocities so that the kinetic effects are treated self-consistently. In general, the linear Vlasov equation is used to derive the thermal damping rates of the waves. Here we use the so-called WHAMP code (Rönmark 1982) for calculation of the damping rate.¹ The diffusion model actually does not distinguish the quasi-2D and wave-like fluctuations (Oughton et al. 2006). The balance between the eddy turnover and wave propagation is

¹Since the damping rate increases sharply with the increase of the wavenumber, the quasi-linear treatment is expected to give a good approximation of the damping even for the nonlinear effect dominated quasi-2D component.

revealed in the diffusion tensor.

We apply our formalism (for cascade and damping) to the Alfvén-cyclotron branch, which has been studied extensively due to its simplicity and its prevalence in magnetized turbulence. It is chosen here to facilitate better comparisons of our models with previous studies. In § 2, we discuss how the turbulence cascade can be studied using the diffusion approximation, which reduces the turbulence evolution to a nonlinear 2D diffusion problem. We also investigate different forms for the diffusion tensor and include wave damping rate. For the simplest cases, where the diffusion tensor is only a function of time, wavevector, and local turbulence power in the wavevector space, the nonlinear diffusion equation can be solved numerically to obtain the power spectrum from the MHD region to the ^4He gyro-frequency, where the Alfvén dispersion surface cuts off. To better understand the cascade models, we first present results for the Alfvén turbulence § 3, where the dispersion relation for Alfvén waves is used. The exact dispersion relation and the cascade beyond the MHD regime are discussed in § 4. The damping effects are investigated in § 5. In § 6 we apply models to solar wind magnetic fluctuations and show that a locally isotropic diffusion model can naturally explain the observations. We discuss the implication of this theory on the study of plasma heating and particle acceleration by magnetized turbulence and future work, and draw conclusions in § 7.

2. Kinetic Equation

Following the approach of Zhou & Matthaeus (1990), we assume local interactions in the wavevector \mathbf{k} space so that the evolution of the turbulence power spectrum $\mathcal{W}(\mathbf{k}, t)$ only depends on its properties near \mathbf{k} at the time t :

$$\frac{\partial \mathcal{W}(\mathbf{k}, t)}{\partial t} = \dot{Q}(\mathbf{k}, t) + \frac{\partial}{\partial k_i} \left[D_{ij}(\mathbf{k}, t) \frac{\partial}{\partial k_j} \mathcal{W}(\mathbf{k}, t) \right] - \Gamma(\mathbf{k}, t) \mathcal{W}(\mathbf{k}, t) - \frac{\mathcal{W}(\mathbf{k}, t)}{T_{\text{esc}}(\mathbf{k}, t)}. \quad (1)$$

Here i, j indicate the three bases of the wave vector \mathbf{k} , and the terms on the right-hand-side represent the turbulence generation, cascade (through diffusion), damping, and leakage processes, respectively. The rates of turbulence generation (\dot{Q}), damping (Γ), and leakage (T_{esc}^{-1}) are mostly determined by the properties of the background plasma, whose variation timescales, comparable to the large scale dynamical time, are usually much longer than the turbulence evolution timescales so that the time-dependence of these rates can be ignored. The diffusion tensor $D_{ij}(\mathbf{k}, t)$ can be constructed with the nonlinear timescale $\tau_{\text{NL}}(\mathbf{k}, t)$ associated with the eddy turnover, the wave crossing time $\tau_{\text{W}}(\mathbf{k})$, and the triple correlation time $\tau_3 = (\tau_{\text{NL}}^{-1} + \tau_{\text{W}}^{-1})^{-1}$. The turbulence cascade rate then is defined as $\tau_{\text{cas}}^{-1} \simeq \tau_{\text{NL}}^{-2} \tau_3$, and $D_{ij} \sim k^2 \tau_{\text{cas}}^{-1}$.

More generally, one may also include an advection term to the above equation so that the energy flux in the wavevector space

$$f_i(\mathbf{k}, t) = -D_{ij}(\mathbf{k}, t) \frac{\partial}{\partial k_j} \mathcal{W}(\mathbf{k}, t) + u_i(\mathbf{k}, t) \mathcal{W}(\mathbf{k}, t), \quad (2)$$

where u_i is a velocity field in the wavevector space (Cranmer & van Ballegoijen 2003). This velocity field can be decomposed into a solenoidal \mathbf{u}_s and a compressible component \mathbf{u}_c . The former is divergence-free and can be attributed to the anti-symmetric part of the diffusion tensor $D_{ij}(\mathbf{k}, t)$. The latter is driven by an external potential in the \mathbf{k} space $\Phi(\mathbf{k}, t)$, i.e., $u_{ci} = \partial\Phi/\partial k_i$. The highly non-linear phenomenon of intermittence can also affect the energy diffusion of turbulence. However, intermittence likely results from the non-local nature of interactions in the wavevector space (Boldyrev 2002; Cho et al. 2002). One may partially take into account the effects of this process on the turbulence energy transfer with a nonlinear damping rate [see e.g., Beresnyak & Lazarian (2008)]. In general, the diffusion tensor is a functional of \mathcal{W} . For local interactions in the \mathbf{k} space, it is reduced to a function of \mathbf{k} . In what follows, we will focus on the relatively simple case with $\mathbf{u}_c = 0$, and D_{ij} symmetric and only functions of \mathbf{k} and t , and ignore the cascade and dissipation associated with intermittence.

Without excitation of waves, i.e., $\tau_W = \infty$, the turbulence cascade is well described with the Kolmogorov phenomenology, which assumes an isotropic incompressible fluid with local interactions of eddies in the wavenumber space so that $\tau_{NL} = (\mathcal{W}k^5)^{-1/2}$ and $D_{ij} = \delta_{ij}k^2/\tau_{NL}$, where δ_{ij} is the Kronecker's delta function. For strong turbulence with $\tau_{NL}(\mathbf{k}) \ll \tau_W(\mathbf{k})$, nonlinear processes dominate and one retains the Kolmogorov phenomenology. In the weak turbulence limit, $\tau_{NL}(\mathbf{k}) \gg \tau_W(\mathbf{k})$ and the turbulence may be described as a spectrum of linear wave modes. For fast mode waves in a cold or low beta plasma (i.e., when the Alfvén speed $v_A \gg C_S$, the sound speed), the wave frequency $\omega(\mathbf{k}) \simeq v_A k$, and $\tau_W = \omega(\mathbf{k})^{-1} \ll \tau_{NL} = (\mathcal{W}k^5)^{-1/2}$, $D_{ij} = \delta_{ij}k\tau_{NL}^{-2}/v_A$, and one recovers the IK phenomenology.² For Alfvén waves, $\omega(\mathbf{k}) = v_A k_{\parallel}$, where k_{\parallel} is the component of the wavevector parallel to the large scale magnetic field, wave packets propagate along the mean magnetic field. Since only oppositely directed wave packets can interact (Galtier et al. 2000), $\tau_W \propto k_{\parallel}^{-1}$. Although the weak turbulence approximation may be valid for parallel propagating waves, nonlinear processes always dominate in the perpendicular direction. Therefore the quasi-linear theory for linear wave modes does not give a complete description of the Alfvénic turbulence fluctuations (Oughton et al. 2006).

We are interested in extending the turbulence cascade study beyond the MHD regime by using the general dispersion relation for the Alfvén-cyclotron fluctuations and compress-

²Note that for sound waves in a fluid, $\omega(\mathbf{k}) = C_S k$, one obtains results similar to fast mode waves.

ible plasma waves. The quasi-linear approaches for MHD wave interactions then become extremely complex if not completely unsolvable. On the other hand, the diffusion approximation can provide simple solutions with a prescribed diffusion tensor and may help us to uncover processes beyond the MHD regime. In the following, we will ignore the leakage term in equation (1) and treat the source term as a δ -function at certain large scale. Thus, for the investigation of the evolution of the turbulence power spectrum we only need proper choices of the diffusion tensor D_{ij} and the damping rate Γ .

2.1. Diffusion Tensor

We adopt the recipe given by Zhou & Matthaeus (1990) for the 1D cascade of Alfvén waves caused by the wave-wave resonances and eddy turnovers and generalize it to waves propagating in arbitrary directions with a propagating direction dependent diffusion tensor. The eddy turnover time can be estimated with $\tau_{\text{NL}} = (v_k k)^{-1}$, where the eddy velocity³

$$v_k \simeq (\mathcal{W}k^3)^{1/2} \quad \text{so that} \quad \tau_{\text{NL}} = (\mathcal{W}k^5)^{-1/2}. \quad (3)$$

For the wave crossing time, one must consider the anisotropy of the Alfvén-cyclotron dispersion. Wave packets with a size of $\sim k_{\parallel}^{-1}$ cross each other at the Alfvén speed. We then have $\tau_{\text{W}} \simeq (v_A k_{\parallel})^{-1}$, and the wave propagation effect reduces the triple correlation time from τ_{NL} to τ_3 and gives a cascade rate $\tau_{\text{cas}}^{-1} = \tau_{\text{NL}}^{-2}/(\tau_{\text{NL}}^{-1} + \tau_{\text{W}}^{-1})$.⁴ Then the simplest (locally isotropic) diffusion tensor may be constructed as:

$$D_{ij} \equiv \delta_{ij} \frac{C}{4\pi} k^2 \tau_{\text{cas}}^{-1} = \delta_{ij} \frac{C}{4\pi} \frac{\mathcal{W}k^7}{(\mathcal{W}k^3)^{1/2}k + v_A k \cos \theta} = \delta_{ij} \frac{C}{4\pi} \frac{\mathcal{W}k^6}{v_k + v_A \cos \theta} \quad (4)$$

where C is a dimensionless scaling constant corresponding to the Kolmogorov constant for hydrodynamic turbulence, and θ is the angle between \mathbf{k} and the mean magnetic field: $k_{\parallel} = k \cos \theta$. In what follows we set $C = 1$.⁵ This diffusion tensor is locally isotropic in the wavevector space implying that the energy of a wave packet at \mathbf{k} can spread into its

³Here we have ignored the potential anisotropy of the turbulence. In a more accurate treatment, one also needs to distinguish contributions to the turbulence power spectrum from the velocity and magnetic fields. The eddy velocity should only depend on the turbulence kinetic energy (Galtier 2006).

⁴Note that, following Kraichnan’s argument (1965) for an isotropic Alfvén wave turbulence, Zhou & Matthaeus (1990) obtained $\tau_{\text{W}} = (v_A k)^{-1}$ for their 1D diffusion model, which is appropriate for the isotropic sound and fast mode waves.

⁵ $C = (3/11)(4\pi/C_0)^{3/2} \simeq 5.89$, where $C_0 \simeq 1.62$ is the Kolmogorov constant (Yeung & Zhou 1997). If the eddy speed $v_k = (4\pi\mathcal{W}k^3)^{1/2}$, $C \simeq 1.66$.

neighborhood in the \mathbf{k} space without any preferred directions. The wave propagation effect just reduces the diffusion coefficient. This reduction is higher for waves with higher phase speeds.

In more general cases, the diffusion tensor may not be locally isotropic in the wave vector space due to resonance interactions.⁶ One may construct the parallel and perpendicular components of the diffusion tensor differently. In the perpendicular direction, the turbulence cascade is determined by the eddy turnover time only. We have $D_{\perp,\perp} = k^2 \tau_{\text{cas},\perp}^{-1} = k^2 \tau_{\text{NL}}^{-1}$. The wave propagation effect reduces the cascade rate in the parallel direction $\tau_{\text{cas},\parallel}^{-1} = \tau_{\text{NL}}^{-2} / (\tau_{\text{NL}}^{-1} + \tau_{\text{W}}^{-1})$, and the corresponding diffusion coefficient can be written as $D_{\parallel,\parallel} = k^2 \tau_{\text{cas},\parallel}^{-1}$. Thus, we obtain an anisotropic diffusion tensor

$$D_{ij} = \frac{1}{4\pi} \frac{k^2}{\tau_{\text{NL}}} \begin{bmatrix} (1 + \tau_{\text{NL}}/\tau_{\text{W}})^{-1} & 0 \\ 0 & 1 \end{bmatrix}. \quad (5)$$

There are also two choices for the wave interaction timescale. We can choose

$$\tau_{\text{W}}^{-1} = \mathbf{k} \cdot \mathbf{v}_{\text{gr}}, \quad \text{or} \quad \omega(\mathbf{k}), \quad (6)$$

where \mathbf{v}_{gr} is the wave group velocity. In the MHD regime they both give $\tau_{\text{W}} = kv_A \cos \theta$ used in equation (4). However, as mentioned above we are often interested in acceleration of low energy particles, which requires cascade to high values of k regime. In this case we should use the exact dispersion relation, going beyond the MHD regime ($k \geq \Omega_p/v_A$), where the above timescales are different. In what follows we will present results for both tensors. A brief review of the exact dispersion relation and its decomposition into different modes is presented in Appendix A. Figure 13 gives the $\omega - k$ relation for different modes at various angles of propagation with respect to the large scale magnetic field.

So far we have only used the dispersion relation of waves to construct the diffusion tensor. Physically the polarization state (including the compressibility) of the waves may also affect the wave diffusion. An equation for the magnetic helicity spectrum is also required (Galtier 2006). These may become more significant when we consider the couplings between different wave branches. They may also explain the weak couplings between incompressible Alfvén wave modes and the compressible fast and slow mode waves (Cho & Lazarian 2003), and the relatively strong couplings between parallel propagating Alfvén and fast mode waves (Chandran 2005). Instead of exploring more possibilities on the forms of the diffusion tensor, we defer to observations of turbulence spectrum in solar winds to point us the right direction. The detailed discussions on this is given in § 6 below.

⁶Non-resonance interactions presumably lead to an isotropy.

2.2. Damping Rate

MHD turbulence in collisionless plasmas is subject to damping caused by both resonance and non-resonance processes. The latter may be associated with current sheets and is not well understood (Leamon et al. 2000; Markovskii et al. 2006), and the former likely dominates the damping of plasma waves (Cho & Lazarian 2006). It is well-known that charged particles can extract energy from plasma waves through cyclotron resonances, transit-time damping (TTD), and Landau damping (LD) processes. Cyclotron resonances by low energy background particles can only lead to damping of a high frequency wave with the wave frequency comparable to the particle gyro-frequency. Magnetic field fluctuations in the direction of the mean magnetic field are required for the TTD processes to operate. The TTD conserves the magnetic moment of the particles. Efficient pitch angle scattering of the particles is also needed for this process to energize particles effectively (Miller 1997). The LD is related to electric field fluctuations along the mean magnetic field and therefore can be very efficient (Stix 1962). Alfvén waves in the MHD regime don't have electric and magnetic field components along the mean magnetic field and therefore are only subject to cyclotron damping by relatively high energy particles, whose gyro-frequency is relatively low. At small scales and/or high frequencies, where the kinetic effects become important, there are electric and magnetic field fluctuations along the mean magnetic field, and the TTD and LD processes can damp the Alfvén wave branch.

The damping of waves energizes the plasma either by heating it or by production of nonthermal tails. The properties of the turbulence and background plasma determine the energy partition into these two channels. Therefore, in general, both the hot plasma and non-thermal particles contribute to the damping rate. Unfortunately there is very little work on determination of the damping rate by nonthermal particles. The only result we are aware of is that by Petrosian et al. (2006) [see also Yan et al. (2008)] on the TTD of fast mode waves in low beta plasmas; $\beta_p < 1$. This was done by using the fact that the rate of particle acceleration and the damping rate are related via the energy conservation (Miller & Roberts 1995; Miller et al. 1996). It was shown that for typical solar flare conditions, except for very large flares, the damping is usually dominated by thermal particles. We believe that the same is also true in the solar wind, where we apply our formalism in this paper, as indicated by the relatively low energy content of non-thermal particles. Thus, in what follows, we include damping by thermal particles only, in which case the damping rate as a function of wavevector \mathbf{k} is given by the imaginary part of the frequency obtained from the dispersion relation for a warm ($T \neq 0$) plasma.

For thermal background particles with isotropic pitch angle distributions, depending on the background magnetic field, particle abundances and temperatures, the different damping

processes of the Alfvén wave branch mentioned above dominate in different wave propagating directions (Gary & Borovsky 2004). At low values of $k_{\parallel} < \Omega_{\alpha}/v_A$, where Ω_{α} is the non-relativistic gyro-frequency of the α -particle, these waves are called the kinetic Alfvén waves (KAW) near $k_{\perp}\rho_p \sim 1$, where ρ_p is the Larmor radius of the thermal background protons. They play important roles in the heating of background particles (Leamon et al. 1999; Cranmer & van Ballegooijen 2005). The quasi-parallel propagating Alfvén waves have very weak electric and magnetic field fluctuations along the large scale magnetic field and therefore are not subject to the TTD and LD. These waves play important roles in the selective acceleration of background ions with different gyro-frequencies to high energies through cyclotron resonances (Reames et al. 1994; Mason et al. 2002; Liu et al. 2004, 2006).

Swanson (1989) gives a simplified expression for the damping rate by electron cyclotron resonances of parallel propagating waves under the weak damping approximation. This result can be easily generalized to calculate the cyclotron damping rate by all background particle species:

$$\frac{\omega_i}{\omega_r} = - \frac{\sum_s \frac{\sqrt{\pi}\omega_{p,s}^2}{\omega_r k v_{t,s}} \exp\left[-\left(\frac{\omega - \epsilon_s \Omega_s}{k v_{t,s}}\right)^2\right]}{\frac{2k^2}{\omega^2} + \sum_s \frac{2\omega - \epsilon_s \Omega_s}{\omega(\omega - \epsilon_s \Omega_s)^2} \omega_{p,s}}.$$

Here subscripts i and r refer to the imaginary and real parts, s stands for different particle species and ω_p , Ω , v_t , and ϵ are the corresponding particle plasma frequency, non-relativistic gyro-frequency, thermal speed, and sign of the charge, respectively. For a given power spectrum of quasi-parallel propagating waves, this equation can be used to study the relative acceleration of different background particle species.

We use the Waves in Homogeneous Anisotropic Multitemperature Plasma (WHAMP) code Rönmark (1982) to obtain the thermal damping rate numerically. When $\Gamma = \omega_i \sim \omega_r$, the weak damping approximation is invalid and the code fails to converge. We use a power-law extrapolation with respect to the wavevector to approximate the damping rate in the strong dissipation regime. This does not affect our result because the turbulence spectra usually cut off at the wavevectors where the damping rate is still much lower than the wave frequency. For further details see Appendix B and Figures 5 and 6 below.

3. Cascade of Alfvén Turbulence

In this section we consider the cascade in the *inertial range* ignoring damping and leakage. To compare with previous studies, we first consider Alfvén turbulence in the MHD

regime with $\tau_W^{-1} = \omega(\mathbf{k}) = k_{\parallel}v_A$. In the strong turbulence limit one has $v_k \gg v_A$ and $\tau_{NL} \ll \tau_W$. As a result the diffusion tensors of equations (4) and (5) lead to the isotropic Kolmogorov cascade. However, in the weak turbulence limit, i.e., $v_k \ll v_A$, they are different from the isotropic IK phenomenology due to the dependence of the Alfvén wave crossing time on the angle of propagation θ . Since the Alfvén wave crossing time τ_W is much longer in the perpendicular direction than in the parallel direction, the wave cascade rate is high in the perpendicular direction and decreases dramatically with the increase of k_{\parallel} . We solve the 2D time-dependent wave kinetic equation (1) with the alternative direction implicit scheme on a uniform log-log grid and with

$$\begin{aligned} \dot{Q}_{\mathcal{W}}(\mathbf{k}, t) &= F_0 \delta(\mathbf{k} - \mathbf{k}_0) \Theta(t), \\ k_{\parallel,0} &= k_{\perp,0} = k_0 = 1.6 \times 10^{-8} \Omega_p / v_A, F_0 = 9.55 \times 10^{-10} v_A^2 \Omega_p, \end{aligned} \quad (7)$$

where Θ is the Heaviside step function and δ is the 3D Dirac- δ -function. A reflective boundary condition is used at the large scale boundary $k_{\parallel,0}, k_{\perp,0}$. In this section, we ignore the damping and leakage and allow the turbulence to escape freely at the high end boundary of k .⁷ Because no damping is included, the time unit is set by the proton gyro-frequency Ω_p . The turbulence power spectral contours obtained with this method are shown in Figure 1 for the two diffusion tensors [eqs. (4) and (5)] at two different times. Figure 2 shows the corresponding steady-state spectral contours (left panels) and power spectra at several propagation angles (right panels).

As expected, the turbulence cascade in the parallel direction is initially suppressed. The Alfvén wave period at the injection scale is given by $T_A = 2\pi/k_{\parallel,0}v_A = 3.9 \times 10^8 \Omega_p^{-1}$. It takes less than $10 T_A$ for the turbulence to reach the small scale boundary of the simulation domain. Steady-states are reached in about $10 T_A$. This result is in conflict with simulations by Cho et al. (2002), where the turbulence power spectrum at a given k_{\perp} is found cutting off exponentially with the increase of k_{\parallel} in the steady-state (Cho et al. 2002). It is not obvious to us what prevents the generation of waves in these simulations. Theoretically, if the turbulence cascades toward small scales following the critical balance proposed by Goldreich & Sridhar (1995), as confirmed by these simulations, it should be able to reverse cascade along lines (surfaces) of constant perpendicular wavenumbers through three wave-interactions. Our time-dependent numerical results in Figure 1 mimic such a reverse cascade process. Over a period of less than T_A (from the left panels to the right ones), high frequency nearly parallel propagating waves are generated by small scale fluctuations of the (quasi-

⁷When damping is included (see § 5 below), it dominates the cascade at high values of k (or small scales). We then choose an upper boundary for k large enough such that all injected wave energy is damped within the simulation domain.

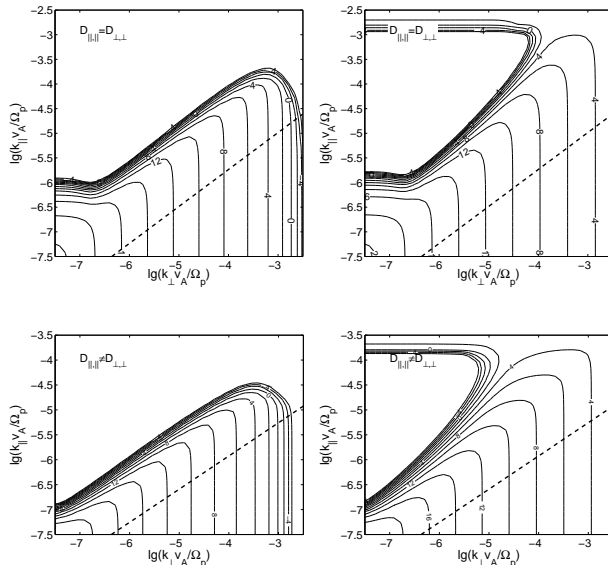


Fig. 1.— Contours of the power spectrum $\mathcal{W}(k_{\parallel}, k_{\perp}, t)$ of the MHD range Alfvén turbulence without damping at $t = 3.46 \times 10^9 \Omega_p^{-1}$ (top left), $3.70 \times 10^9 \Omega_p^{-1}$ (top right), $1.16 \times 10^9 \Omega_p^{-1}$ (bottom left), and $1.26 \times 10^9 \Omega_p^{-1}$ (bottom right). The energy is injected uniformly at the surface of $k_{\parallel,0} = k_{\perp,0} = 1.6 \times 10^{-8} \Omega_p / v_A$ with an injection rate $F_0 = 9.55 \times 10^{-10} v_A^2 \Omega_p$. The logarithm to the base 10 of the contour levels in units of $v_A^5 \Omega_p^{-3}$ are indicated in the figures. The upper and lower panels show the results of the isotropic ($D_{\parallel,\parallel} = D_{\perp,\perp}$) and anisotropic ($D_{\parallel,\parallel} \neq D_{\perp,\perp}$) diffusion models, respectively. The dashed lines indicate the critical balance relation discussed in the text. The power spectra in the left panels are similar to those uncovered by MHD simulations (Cho et al. 2002). The reverse cascade in the perpendicular direction at high values of k_{\parallel} is evident in the right panels.

2D) perpendicular component. This phenomenon is caused by the increase of the diffusion coefficient with the increase of the wavenumber and the suppression of the diffusion toward small parallel scales. At large scales, the wave energy can also diffuse slowly toward high values of k_{\parallel} .

3.1. Results from Isotropic Diffusion Tensor

Let us first consider the *locally* isotropic diffusion tensor (top panels). Note that the magnetic Mach number $M_A = v(k_0)/v_A = 0.30$, which means that our numerical solution is in the wave effect dominant domain. The steady-state power spectrum is nearly isotropic and is very similar to the IK spectrum between $10^{-6} \Omega_p / v_A$ and $10^{-3} \Omega_p / v_A$, $\mathcal{W} = \mathcal{W}_0 (k/k_0)^{-7/2+\alpha}$,

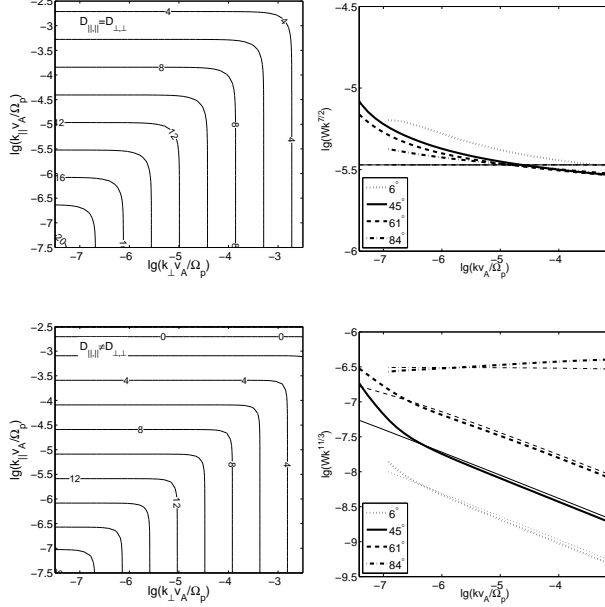


Fig. 2.— *Left:* Same as Figure 1 but for the steady-state power spectral contours. *Right:* The scaled steady-state power spectra in several propagation directions indicated in the legends. The Alfvén Mach number $M_A = 0.30$ for the top panels and $M_A = 0.23$ for the bottom panels. The thick lines in the right panels are simulation results. The isotropic diffusion coefficient produces a nearly isotropic spectrum, which is very similar to the isotropic Kraichnan spectrum (thin horizontal lines), and the anisotropic diffusion coefficient produces spectra steeper than the Kolmogorov spectrum in directions other than the perpendicular direction. The thin straight lines (power-laws) are the approximate spectra based on equation (17). The spectral features at low values of k may depend on the geometry of the surface, where energy is injected into the system.

where $\alpha(k) \ll 1$ is a slowly varying function of wavenumber k ($\alpha(k \rightarrow \infty) \rightarrow 0$). Substitution of this spectrum and D_{ij} given in equation (4) into equation (2) gives, the radial component of the slightly anisotropic energy flux density as

$$f(k) = (1/4\pi)(7/2 - \alpha - k\alpha' \ln(k/k_0))\mathcal{W}^2 k^5 [v_k + v_A \mu]^{-1}, \quad (8)$$

where $\mu = \cos \theta$ and the prime indicates derivative with respect to k . The total energy flux through spheres centred at the origin of the \mathbf{k} space is then

$$\begin{aligned} F_0 &= (7/2 - \alpha - k\alpha' \ln(k/k_0))\mathcal{W}^2 k^7 \int_0^1 d\mu [(v_k + v_A \mu)^{-1}] \\ &= (7/2 - \alpha - k\alpha' \ln(k/k_0))\mathcal{W}^2 k^7 v_A^{-1} \ln[1 + v_A/v_k], \end{aligned} \quad (9)$$

which should be independent of k in the steady-state case.⁸

For a nearly isotropic solution, the constancy of F_0 can be used to derive the weak dependence of α on k :

$$7/2 - \alpha(k) - k\alpha' \ln(k/k_0) = F_0 v_A / [\mathcal{W}^2 k^7 \ln(1 + v_A/v_k)] \quad (10)$$

and the radial energy flux density becomes

$$f = \frac{F_0}{4\pi k^2 (v_k/v_A + \cos\theta) \ln(1 + v_A/v_k)}, \quad (11)$$

which deviates from the k^{-2} dependence expected for exactly isotropic solutions for $M_A < 1$, especially near the perpendicular directions. So there is no exactly isotropic solution for this diffusion tensor.⁹ The steady-state solution we get here is just approximately isotropic, and there is no feature associated with the critical balance proposed by Goldreich & Sridhar (1995). It is similar to the steady-state fast mode solution given by Chandran (2005) for coupled weak Alfvén-fast mode turbulence. As expected, for $v_k \gg v_A$, $f = F_0/4\pi k^2$, the turbulence is isotropic.

On the other hand, in the wave effect dominant regime if we assume an isotropic power-law spectrum with $\alpha = 0$, the Alfvén wave crossing process starts to affect the wave cascade at $k_{\parallel} \propto k^{3/4}$, which is similar to the critical balance relation described by Goldreich & Sridhar (1995) and explains the $k_{\parallel} \propto k^{3/4}$ scaling of the cascading wavevector front in the time-dependent power spectrum (Fig. 1). This cascading wavevector front extends until it

⁸Note that the IK spectrum ($\mathcal{W} \propto k^{-7/2}$) does approximately satisfy this constraint for $v_A \gg v$, and for $v \gg v_A$,

$$F_0 \simeq (7/2 - \alpha - k\alpha' \ln(k/k_0)) \mathcal{W}^{3/2} k^{11/2},$$

one recovers the Kolmogorov spectrum.

⁹For locally isotropic diffusion tensors with their dependence on the wavenumber and the wave propagation direction separable, one can always find an isotropic solution for the steady-state power spectrum in the inertial range (Chandran 2005). In this case, the diffusion equation can be simplified as

$$4\pi k^2 D(\mathbf{k}, k, \mathcal{W}) \frac{d\mathcal{W}(k)}{dk} = F_0(\mathbf{k}/k), \quad (12)$$

where F_0 gives the steady-state radial energy flux and is independent of k in the inertial range. Let $F_0(\mathbf{k}/k)$ have the same propagation direction dependence as D , the corresponding formal solution is then given by

$$\mathcal{W}(k) = \int^k dk F_0(\mathbf{k}/k) k^{-2} [4\pi D(\mathbf{k}/k, k, \mathcal{W})]^{-1}. \quad (13)$$

reaches the numerical boundary or the physical limit set by damping or non-MHD effects at large k . Because our eddy turnover timescale has different k and \mathcal{W} dependence's than that given by Goldreich & Shridhar (1995), we obtain a different critical balance relation. For $\mathcal{W} \propto k_{\perp}^{-11/3}$ with $v_k^2 = \mathcal{W}k_{\perp}^3$ and $\tau_{\text{NL}} = (v_k k_{\perp})^{-1}$, one can recover the Goldreich & Shridhar critical balance relation $k_{\parallel} \propto k_{\perp}^{2/3}$.

The critical propagation direction, which separates the linear and nonlinear effect dominant regimes, satisfies $\cos \theta_c = v_k/v_A \propto (k/k_0)^{-1/4}$. Although the cascading energy flux is highly concentrated in the perpendicular directions with small values of k_{\parallel} , the diffusion process eventually carries wave energy to large values of k_{\parallel} . The turbulence fills all possible wavevector space in the steady-state. The fraction of energy, which becomes linear Alfvén waves, is given by the wave efficiency

$$\eta_{\text{W}} = \int_{\cos \theta_c}^1 f d\mu / \int_0^1 f d\mu = 1 - \ln 2 / \ln[1 + v_A/v_k], \quad (14)$$

which approaches 1 as $k \rightarrow \infty$. So the wave like component dominates at small scales as expected from the scalings of the cascade and wave crossing timescales with k mentioned above.

When $v_k \geq v_A$, $\eta_{\text{W}} \leq 0$ and the above formula for the wave efficiency is invalid. The turbulence then is dominated by nonlinear effects. One therefore can define a transition wave number k_{tr} so that $v(k_{\text{tr}}) = [\mathcal{W}(k_{\text{tr}})k_{\text{tr}}^3]^{1/2} = v_A$. Then

$$\mathcal{W}(k, F_0, v_A) \simeq \left(\frac{3F_0}{11}\right)^{2/3} k_{\text{tr}}^{-11/3} (k/k_{\text{tr}})^{-7/2+\alpha} \simeq v_A^{11} \left(\frac{11}{3F_0}\right)^3 (k/k_{\text{tr}})^{-7/2+\alpha}, \quad (15)$$

where

$$\alpha(k) + k\alpha' \ln(k/k_0) \simeq 7/2 - (11/3)(k_{\text{tr}}/k)^{2\alpha} / \ln[1 + v_A/v_k] \quad (16)$$

and $k_{\text{tr}} \simeq 3F_0/11v_A^3$. We note that $\alpha \rightarrow 0$ for $k \gg k_{\text{tr}}$ or $v_k \ll v_A$ (IK spectrum), and $\alpha \rightarrow -1/6$ for $k \ll k_{\text{tr}}$ or $v_k \gg v_A$ (Kolmogorov spectrum). The transition scale is proportional to the cube of the Alfvén velocity and inversely proportional to the energy injection rate. It gives the coherent length of the magnetic field (Cho & Vishniac 2000) and may determine the maximum energy that charged particles can reach through resonant interactions with the turbulent magnetic field (Liu et al. 2008). The top right panel of Figure 2 compares the numerical results with the IK spectrum, $\mathcal{W}(k, F_0, v_A) \simeq 0.22v_A^{11} (11/3F_0)^3 (k/k_{\text{tr}})^{-7/2}$ (thin solid line). The deviations of the spectra in different wave propagation directions from the IK spectrum at $k < 10^{-6}\Omega_p/v_A$ shown in Figure 2 are likely caused by the cylinder geometry of the surface with $k_{\parallel 0} = k_{\perp 0} = k_0 = 1.6 \times 10^{-8}\Omega_p/v_A$, where turbulence energy is injected into the system. For the parameters of this numerical calculation, $k_{\text{tr}} = 2.60 \times 10^{-10}\Omega_p/v_A$, and equation (15) with $\alpha = 0$ predicts an $M_A = (k_{\text{tr}}/k_0)^{1/4} \simeq 0.36$ at $k_0 = 1.6 \times 10^{-8}\Omega_p/v_A$, which is in agreement with the numerical results.

3.2. Results from Anisotropic Diffusion Tensor

For the *locally* anisotropic diffusion tensor (5) the diffusion coefficient in the perpendicular direction is higher than that of the isotropic diffusion model. Thus, for a given energy injection rate, in the steady-state case, the turbulence contains slightly less energy than that of the isotropic model. We find that for $M_A = 0.23$, the steady-state power spectral contours (Fig. 2, bottom panels) can be fitted with

$$\mathcal{W}(\mathbf{k}) \simeq 0.62 \left(\frac{3F_0}{11} \right)^{2/3} k_{tr}^{-11/3} \left[\left(\frac{k_{||}}{k_{||,tr}} \right)^{\alpha_{||}} + \left(\frac{k_{\perp}}{k_{\perp,tr}} \right)^{\alpha_{\perp}} \right]^{-\alpha} \quad (17)$$

with $\alpha = 1$, $\alpha_{\perp} = 11/3$, $\alpha_{||} = 4$, $k_{||,tr} = 0.5k_{\perp,tr}$, and $k_{tr} = (k_{||,tr}^2 + k_{\perp,tr}^2)^{1/2} \simeq 3F_0/11v_A^3$. The bottom right panel of Figure 2 compares this analytical fit (thin lines) to the numerical results (thick lines). The significant differences between the fit and numerical results at low values of k may also be related to the assumed cylindrical geometry of the injection surface. As evident for $\theta \sim \pi/2$ we have a spectrum very similar to the Kolmogorov spectrum, but away from the transverse direction the spectrum at high k 's becomes $\propto k^{-4}$ very quickly. In the limit of $k \gg k_{tr}$, the angle averaged spectrum $W(k) \equiv \int \mathcal{W}(\mathbf{k}) k^2 d\Omega \propto k^{1-\alpha\alpha_{\perp}+\alpha_{\perp}/\alpha_{||}} = k^{-7/4}$. These results are similar to Chandran's steady-state solutions, but there are significant quantitative differences. The corresponding critical balance $v_A k_{||} = v_k k$ leads to

$$k_{||} = 0.79 k_{tr}^{1/3} k_{\perp}^{-11/6} k^{5/2} [1 + 2^{11/3} (k_{||}/k_{\perp})^4 (k_{\perp}/k_{||,tr})^{1/3}]^{-1/2} \simeq 0.79 k_{tr}^{1/3} k_{\perp}^{2/3}. \quad (18)$$

This is almost identical to the critical balance relation proposed by Goldreich & Sridhar (1995).¹⁰ The spectrum of the nonlinear effect dominant 2D component $W_{2D}(k_{\perp}) \equiv 2\pi k_{\perp} \int_{v_A k_{||} < v_k} \mathcal{W}(\mathbf{k}) dk_{||} k_{\perp}^{-2}$, which is different from the result of Goldreich & Sridhar (1995). As for the isotropic case, this is due to the difference in the scaling of the eddy turnover timescale with \mathbf{k} and \mathcal{W} . In our model $v_k^2 \propto \mathcal{W} k^3$, while $v_k^2 \propto \mathcal{W} k_{||} k_{\perp}^2$ in Goldreich & Sridhar model. The fact that the spectrum of the 2D component is softer than the overall turbulence spectrum is also consistent with the assessment that the wave component dominates at small spatial scales. The energy flux of the 2D component $F_{2D}(k_{\perp}) \equiv 2\pi k_{\perp} \int_{v_A k_{||} < v_k} D_{\perp,\perp} [\partial \mathcal{W}(\mathbf{k}) / \partial k_{\perp}] dk_{||} \propto k_{\perp}^{-1/3}$, which decreases with k_{\perp} , and as the turbulence cascades towards small spatial scales, there is continuous energy conversion from the 2D perpendicular component to the wave component.

On the other hand, based on the anisotropy of the steady-state spectrum, one may define a perpendicular component of the turbulence with $k_{\perp}/k_{\perp,tr} > k_{||}/k_{||,tr}$, the corresponding spectrum $W_{\perp}(k_{\perp}) \equiv 2\pi k_{\perp} \int_{k_{\perp}/k_{||,tr} > k_{||}/k_{\perp,tr}} \mathcal{W}(\mathbf{k}) dk_{||} \propto k_{\perp}^{-5/3}$. Due to the anisotropy of the diffusion tensor, this component develops quickly as can be seen from the time-dependent results

¹⁰The critical balance only exists in the regime of $v_k \ll v_A$, which implies $k_{||} \ll k \simeq k_{\perp}$.

(Fig. 1). The perpendicular energy flux $F_{\perp}(k_{\perp}) \equiv 2\pi k_{\perp} \int_{k_{\perp} k_{\parallel, tr} > k_{\parallel} k_{\perp, tr}} D_{\perp, \perp}[\partial \mathcal{W}(\mathbf{k})/\partial k_{\perp}] dk_{\parallel} \propto k_{\perp}^{-1/3}$, which also carries most of the energy flux from large scales to small scales. The corresponding parallel component with $k_{\perp}/k_{\perp, tr} < k_{\parallel}/k_{\parallel, tr}$ is dominated by linear waves and has a much steeper spectrum $W_{\parallel}(k_{\parallel}) \equiv \int_{k_{\perp} k_{\parallel, tr} < k_{\parallel} k_{\perp, tr}} 2\pi k_{\perp} \mathcal{W}(\mathbf{k}) dk_{\perp} \propto k_{\parallel}^{-2}$. The parallel energy flux $F_{\parallel}(k_{\parallel}) \equiv \int_{k_{\perp} k_{\parallel, tr} < k_{\parallel} k_{\perp, tr}} 4\pi k_{\perp} D_{\parallel, \parallel}[\partial \mathcal{W}(\mathbf{k})/\partial k_{\parallel}] dk_{\perp} \propto k_{\parallel}^{-1}$. Since both the perpendicular and parallel energy fluxes decrease with the increase of k , the total energy is not conserved, which reflects the inaccuracy of the analytical fit to the numerical results (Fig. 2). The energy is better conserved with a slightly higher value of α_{\perp} . Instead of pursuing even better analytical fits to the steady-state spectrum, which most likely will be complicated, we focus on numerical results in what follows.

The most notable difference between these results and recent theoretical and numerical studies of Alfvén turbulence is the presence of a prominent parallel wave component in our model. Such a component is found to be absent or dynamical unimportant in many studies (Galtier 2006; Cho et al. 2002; Goldreich & Sridhar 1995). On the other hand, these parallel wave modes may play a dominant role in the selective acceleration of ions from the background plasma (Mason et al. 2002; Liu et al. 2004, 2006) and scattering of high energy particles. They have been the subject of extensive studies (Yan & Lazarian 2002; Farmer & Goldreich 2004; Lazarian & Beresnyak 2006). Since the diffusion process tends to fill the wave vector space with energy, the presence of a strong parallel wave component is not a surprise in our model. They are also not subject to the turbulence damping studied by Farmer & Goldreich (2004) and Lazarian & Beresnyak (2006). This damping is caused by the interactions of the waves with the quasi-2D strong turbulence component in the perpendicular direction, which makes the waves cascade toward small perpendicular scales. Our parallel wave component is produced by the cascade (or reverse cascade) itself. So the cascade process generates these waves instead of damping them. With the strong turbulence theory proposed by Goldreich & Sridhar (1995), high values of k_{\parallel} can be reached through the critically balanced cascade $k_{\parallel} \propto k_{\perp}^{2/3}$. The turbulence power spectrum is given by $W \propto k_{\perp}^{-10/3} g(k_{\parallel}/k_{\perp}^{2/3})$. If the turbulence can cascade along lines of constant values of k_{\perp} as required by the three-wave resonance conditions, one would expect that at a given value of k_{\parallel} , the spectrum is flat with the increase of k_{\perp} until the critical balance condition is satisfied. Therefore $W \propto k_{\perp}^{-10/3} \propto k_{\parallel}^{-5}$. This result is similar to the result of our anisotropic cascade model. However, they are quite different from the power spectrum derived from MHD simulations by Cho et al. (2002), where it is found that the spectra cut off exponentially toward small parallel scales. It remains to be seen what prevents the presence of the parallel wave component in these simulations.

4. Turbulence Cascade beyond the MHD Regime

So far we have assumed the simple MHD dispersion relation $\omega = kv_A \cos \theta$, which is valid on large scales. For a more exact treatment of both cascade and damping we need to go beyond the MHD regime and use a more complete description of the dispersion relation, which is well known. Linear waves in collisionless magnetized plasmas have been studied extensively with the linear Vlasov theory (André 1985). Here, for the purpose of comparing with the observed turbulence in the solar wind, we focus on the dominant Alfvén-cyclotron fluctuations. Observations suggest that the Alfvén turbulence can cascade to spatial scales below the MHD regime and the kinetic effects are important (Denskat et al. 1983; Leamon et al. 1998, 1999; Bale et al. 2005; Osman & Horbury 2007). For fully ionized plasmas with the solar abundance, the dispersion relation deviates from the simple MHD relation significantly near the ^4He nucleus (or α -particle) cyclotron frequency $\Omega_\alpha = 0.5\Omega_p = 0.076(2\pi)(B/10\text{nT})\text{Hz}$ (the Alfvén-cyclotron fluctuations exist only below this frequency).

Our diffusion tensor is constructed from the wave dispersion relation $\omega_r(\mathbf{k})$, where the subscript “ r ” refers to the real part of the frequency. (As discussed in §2.2 and below, the imaginary part determines the damping rate.). For an accurate determination of ω_r we use the WHAMP code to obtain the “hot-plasma” Alfvén wave dispersion surface (Rönnmark 1982). The thin lines in Figure 3 show this relation for different angles of propagation under typical solar wind conditions (temperature $T \sim 4 \times 10^4$ K). These match very closely the “cold plasma” ($T = 0$) dispersion relation, shown by the thick lines (see Appendix A), up to $k \sim 0.6\Omega_p/v_A$ with less than 30% deviation at highest frequencies.¹¹ At a higher (lower) values of temperature the deviation will start at a lower (higher) value of k . In what follows we use the cold plasma dispersion relation without loss of much accuracy but with a great gain in computational simplification because these dispersion relations can be described analytically. This greatly simplifies the construction of the diffusion tensor at all the wavevector grid points.

For Alfvén waves, the turbulence cascades preferentially in the perpendicular direction. This is still true when we consider the kinetic effects on the plasma wave dispersion relations. However, as mentioned above in the MHD regime the Alfvén waves have a well defined wave crossing time. The kinetic effects introduce ambiguities on the definition of τ_W . One therefore can identify τ_W^{-1} with either $\omega_r(\mathbf{k})$ or $\mathbf{v}_{\text{gr}} \cdot \mathbf{k}$. Because the Alfvén wave packet becomes

¹¹Note that the hot plasma dispersion curves terminate at some finite values of k . This is because currently there are no simple schemes, which can lead to reliable dispersion relation (and damping rate) in the high frequency range, where damping dominates the wave effect. At such high frequencies thermal damping dominates and, as we will see below, the turbulence spectrum cuts off sharply.

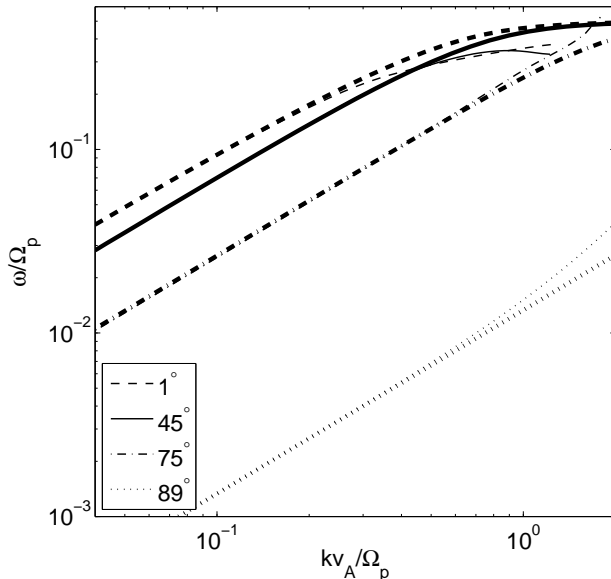


Fig. 3.— Dispersion relations (the real part of the wave frequency) of Alfvén-cyclotron fluctuations in several wave propagation directions. The thick lines give the cold plasma relations and the thin lines are obtained numerically with the WHAMP code. We assume $\Omega_p = 0.096(2\pi)$ Hz ($B = 6.3$ nT), the electron and ions temperatures $k_B T_e = k_B T_p = k_B T_\alpha = 3.35$ eV, and densities $n_e = 12$ cm $^{-3}$ ($\beta_p = 0.41$), $n_p = 10$ cm $^{-3}$, $n_\alpha = 1$ cm $^{-3}$, which are typical for the solar wind (Leamon et al. 1998, 1999). Note that the Lauren series are used in the code to approximate the plasma dispersion function Z , that is valid when the damping rate, i.e., the imaginary part of the wave frequency $\omega_i = \Gamma$, is much less than the real wave frequency ω_r . Thus, the solution at high frequencies may not be valid. The missing segments of the dispersion relation in the figure are related to this caveat.

stationary near Ω_α (where $k \rightarrow \infty$), one may favor the latter choice that implies negligible wave propagation effects. It is not obvious which one of these two choices is physically more reasonable. We first try both forms still without the damping (or leakage) term. The corresponding steady-state spectra are shown in Figure 4. The spectra are nearly identical at large scales (the spectra for $\tau_W^{-1} = \omega$ are shifted upward by a factor of 5 for the illustrative purpose) and, as expected, both contain a spectral break at $k_{\parallel} v_A \sim \Omega_\alpha$, where the wave dispersion surface starts to deviate from the MHD relation. These breaks, though appealing, only have a spectral index change of less than one. They may explain a few observations of solar wind turbulence (Bale et al. 2005). However, neither of these breaks can account for the more commonly observed steep spectra at high frequencies (Denskat et al. 1983; Leamon et al. 1998; Cranmer & van Ballegooijen 2003; Osman & Horbury 2007). In the

kinetic effect dominant regime, the wave propagation effects vanish for $\tau_W^{-1} = \mathbf{v}_{\text{gr}} \cdot \mathbf{k}$, the spectra approach, once again, the Kolmogorov spectrum at high values of k .

We will show below (§ 5) these two cases cannot be distinguished with most observations of the solar wind turbulence since the strong thermal damping cuts off the spectra at the wavevectors before the spectral deviations due to the kinetic effects shown above set in. [For other conditions, e.g., with lower temperatures, the break due to kinetic effects may appear before the damping cuts off the spectra, see e.g., Bale et al. (2005).] The kinetic effects, however, play crucial roles in the thermal damping processes. In what follows, we leave the subtle differences between these two possible choices of the wave coupling times to further study, and adopt the first choice, i.e., $\tau_W = \omega^{-1}$ obtained from the exact cold plasma dispersion relation for both the isotropic and anisotropic diffusion tensors [eqs. (4) and (5)].

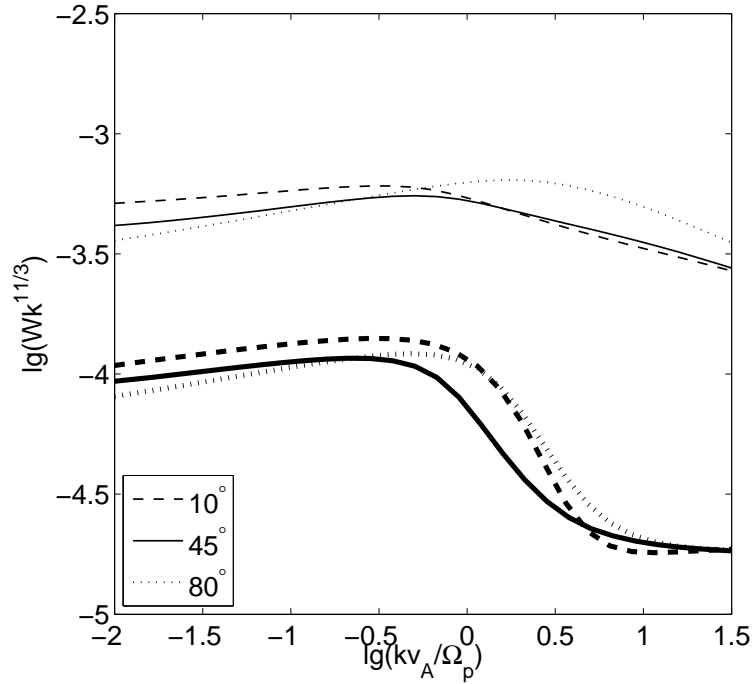


Fig. 4.— The steady-state wave power spectra in several wave propagation directions. The energy is injected at $k_{\parallel 0} = k_{\perp 0} = 2.01 \times 10^{-4} \Omega_p / v_A$ with $\mathcal{W}(\mathbf{k}_0) = 1.44 \times 10^9 v_A^5 \Omega_p^{-3}$. The corresponding Mach number $M_A = 0.18$. The upper and lower lines are for $\tau_W^{-1} = \omega_r(\mathbf{k})$ and $\mathbf{k} \cdot \mathbf{v}_{\text{gr}}$, respectively. To avoid confusion the former has been shifted upward by a factor of 5. The spectral breaks at $k_{\parallel} v_A \simeq 0.5 \Omega_p$ in both cases are due to the kinetic effects on the wave dispersion relation.

5. Turbulence Spectra in the Dissipation Range

It is well-known that the damping of waves in a magnetized plasma by thermal background particles is not isotropic (Gary & Borovsky 2004). In combination with the anisotropy of the turbulence cascade, we would expect strong anisotropies in the turbulence spectrum in the dissipation range. These anisotropies have significant effects on the energizing of background particles by turbulent plasma waves and have broad implications on the energy dissipation in collision-less astrophysical plasmas. Although these issues have been well-recognized, there are only preliminary and approximate investigations of the relevant processes (Leamon et al. 1999; Cranmer & van Ballegoijen 2003; Howes et al. 2007, 2008a). Compared with previous studies, our model has less assumptions with most of the related physical processes treated more self-consistently. We present the corresponding results in this section.

5.1. Start of the Dissipation

As mentioned above the damping rate can be calculated from the WHAMP code for a thermal plasma with $\Gamma(\mathbf{k}) = \omega_i(\mathbf{k})$, the imaginary part of the wave frequency. To our knowledge there are no equations or programs for damping by an arbitrary nonthermal particle distributions except the recent result from Petrosian et al. (2006) for the TTD damping of fast mode waves in low beta plasmas. As shown in this paper the damping rate increases with increasing k more rapidly than the cascade rate so that it becomes important beyond some critical wavevector \mathbf{k}_c obtained from $\Gamma(\mathbf{k}_c) = \tau_{\text{cas}}^{-1}(\mathbf{k}_c)$. And one expects sharp cutoff of the turbulence spectrum for $k > |\mathbf{k}_c|$ at a given wave propagation direction, which corresponds to the dissipation range. In what follows we first follow this procedure assuming a thermal plasma to estimate the dissipation range turbulence spectrum and then show exact numerical results from the solution of the wave equation including both the diffusion and damping terms (with the leakage term still ignored).

For the locally isotropic diffusion model, the cascade rate is uniquely defined as $\tau_{\text{cas}}^{-1} = \tau_{NL}^{-1}/(1 + \tau_{NL}/\tau_W)$. The left panel of Figure 5 shows this cascade rate (from the above numerical results with damping excluded) and the thermal damping rate (for the plasma in Figure 3) in several wave propagation directions. We see that with the increase of k the damping rate increases much faster than the cascade rate. The cutoff wave number k_c is given by the intersection of these two rates. The solid line in the middle panel shows the dependence of k_c on θ . The dotted and dashed lines give contours of constant cascade and damping rates, respectively. These anisotropic damping and cascade make k_c change by more than one order of magnitude with the change of the wave propagation direction.

This is distinct from the 1D turbulence model, where the dissipation range covers a very narrow spatial scales with the Reynolds number on the order of 1. The right panel shows the dependence of k_c on β_p and the turbulence intensity. Higher values of β_p lead to stronger damping and lower values of k_c . With the increase of the turbulence intensity, the dissipation range shifts to smaller spatial scales. For the model with the anisotropic diffusion tensor, the cascade rate in the parallel direction is different from that in the perpendicular direction. The model expectations are also more involved. However, numerical evaluations of both models are straightforward.

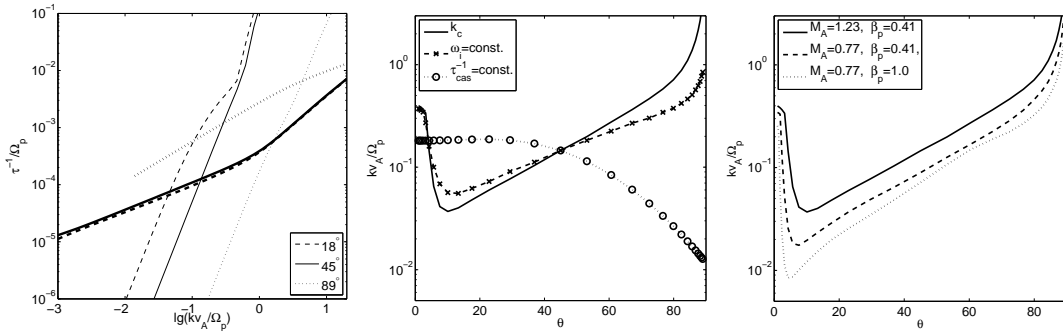


Fig. 5.— *Left*: The wave cascade rates obtained without damping (thick) and damping rates (ω_i , thin) as functions of k for three wave propagation directions. The properties of the plasma are the same as in Figure 3. The energy is injected at $k_{\parallel 0} = k_{\perp 0} = 2.01 \times 10^{-4} \Omega_p / v_A$ with $F_0 = 1.89 \times 10^{-3} v_A^2 \Omega_p$, which implies $\mathcal{W}(\mathbf{k}_0) = 6.62 \times 10^{10} v_A^5 \Omega_p^{-3}$. The corresponding $M_A = 1.23$. *Middle*: The dotted and dashed lines show a sample contour of the above cascade and damping rates in the wavevector space (k, θ), respectively, for $\tau^{-1} = 10^{-4} \Omega_p$. The critical wavenumber k_c defined as the location where these two rates are equal is indicated by the solid line. At a given θ , ω_i increases monotonically with k . The turbulence spectrum should cut off at k_c , which varies by more than one order of magnitude with the change of the wave propagation direction. The nearly parallel propagating waves are damped through cyclotron resonances at $\omega \simeq \Omega_\alpha$. Obliquely propagating waves are subject to the TTD and LD. The nonlinear effects dominate in the nearly perpendicular directions. *Right*: The dependence of k_c on β_p and M_A . Solid, dashed, and dotted lines show the cases with $(M_A = 1.23, \beta_p = 0.41)$, $(M_A = 0.77, \beta_p = 0.41)$, and $(M_A = 0.77, \beta_p = 1.0)$, respectively. With the increase of the turbulence intensity, the cascade rate increases leading to higher values of k_c . The damping rate increases with β_p so that a higher β_p leads to lower values of k_c .

5.2. More Exact Spectra

We now present some numerical results on the spectrum and anisotropy of the turbulence in the dissipation range where we include the thermal damping term using the WHAMP code as described in § 2.2. The left and middle panels of Figure 6 show the steady-state turbulence power spectrum for the isotropic diffusion model. For the plasma parameters chosen here the break due to damping comes before the spectral break associated with the kinetic effects shown in the previous section. We therefore do not expect spectral features caused by the kinetic effects on the turbulence cascade (Stawicki et al. 2001). The spectra cut off sharply when the damping dominates, which is consistent with the results of the previous 1D models (Miller et al. 1995, 1996; Li et al. 2001; Stawicki et al. 2001). This is mainly due to the non-linear nature of the diffusion equation. Once the damping rate is high enough to make the turbulence spectrum deviates significantly from the inertial range spectrum, the cascade, whose rate decreases with the decrease of the local turbulence power in the wavevector space, is suppressed, driving the cascade and damping processes out of balance quickly with the increase of k and resulting in a sharp spectral cutoff. Therefore, it is very difficult to produce a broken-power law spectrum or even a gradual cutoff through the thermal damping with the 1D model except in some unusual scenarios, where the damping processes themselves are also nonlinear and the damping rate scales the same way with k and \mathcal{W} as the cascade rate (Markovskii et al. 2006). We also don't see the gradual spectral cutoff due to the gradual onset of damping with the increase of k as suggested by Gary & Borovsky (2004). Such more gradual cutoffs may appear with different properties of the background plasma (Howes et al. 2008a).

As expected, the actual location of the cutoff wavevector depends on the wave propagation angle. As a consequence of weaker damping and stronger cascade in the perpendicular directions, the perpendicular wave spectra cut off at scales (wavenumbers) about one order of magnitude smaller (larger) than that of the parallel waves. Using the equality of the cascade and damping rates as the criterion for spectral break one would expect strongest damping for waves with $\theta \sim 10^\circ$; the minimum of k_c vs. θ plot (in middle panel of Fig. 5). However, the valley here is smoothed out due to the nature of the diffusion processes. Waves with higher and lower values of θ can cascade to smaller scales and induce waves with $\theta \sim 10^\circ$ through the diffusion processes. The isotropy of the diffusion tensor makes the spectrum of waves subjected to heavy damping cut off at a value higher than k_c . Note also that the cascade rate in Figure 5 is evaluated without the damping. The actual cutoff wavenumber should be lower than k_c in general. The right panel shows the spectral contours for the anisotropic diffusion tensor. The parallel component is damped even more quickly because the turbulence spectrum is dominated by the perpendicular component whose damping sets in within a relatively narrow wavenumber range. The turbulence is therefore strongly anisotropic in

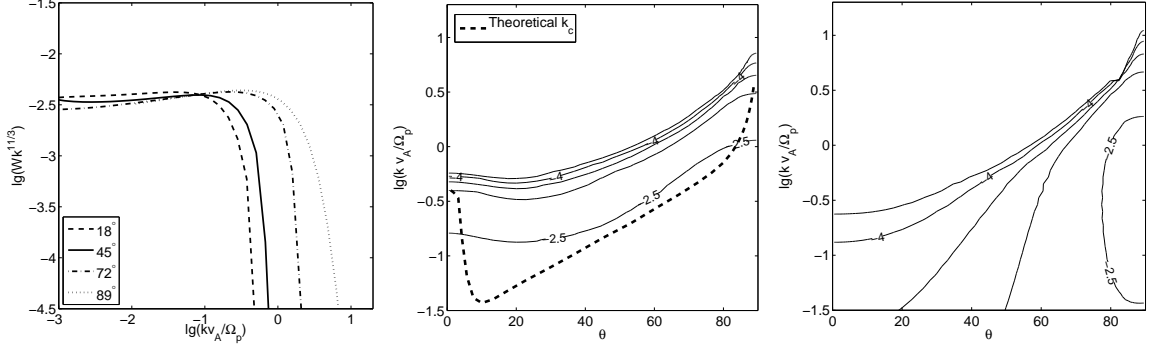


Fig. 6.— *Left*: Same as Figure 4 with the thermal damping included. The turbulence injection and properties of the background plasma are the same as that in the *left* panel of Figure 5. As expected, the power spectrum cuts off sharply at high values of k , and the location of the cutoff wavenumber k_c is very sensitive to the wave propagation direction. *Middle*: The corresponding contours of $\log_{10}(Wk^{11/3})$ (solid lines, starting at -2.5 and decreasing in steps of 0.5) of the *Left* panel in $k - \theta$ plane. The spectrum breaks near -2.5. The dashed line indicates k_c obtained from the prescription given in Figure 5. The diffusion process smoothes out the valley near $\theta = 10^\circ$ in $k_c(\theta)$. *Right*: Same as the *Middle* panel but for the anisotropic diffusion tensor. The turbulence is dominated by the perpendicular component, which is damped over a narrow wavenumber range.

the dissipation range.

5.3. Total Spectra

The angle averaged turbulence spectra are shown in the left (as a function of the wavenumber) and middle (as a function of the frequency) panels of Figure 7. The spectra of the isotropic diffusion model mimic broken-power laws with softer dissipation range spectra. The dissipation range extends nearly one order of magnitude in both wavenumber and frequency, which may explain the observed broken power law spectrum of the solar wind Alfvén turbulence. However, due to the low value of Ω_α , the break frequency is about one order of magnitude lower than the observed value. Although the anisotropic diffusion model has a broader dissipation range as shown in the right panel of Figure 6, due to the dominance of the perpendicular component the angle averaged spectrum can be fitted with a single power law, which cuts off when the damping of the perpendicular component becomes significant. The spectrum of the anisotropic diffusion model therefore appears to cut off much sharply with a narrow dissipation range, which is similar to that of the 1D diffusion

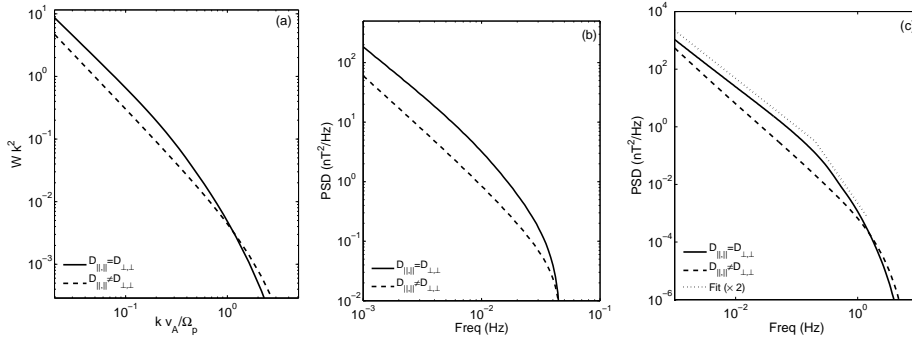


Fig. 7.— *Left*: Angle averaged turbulence power spectra as functions of k for the spectra in Figure 6. The isotropic diffusion tensor (solid) gives a gradual cutoff with the dissipation range covering about one order of magnitude in the wavenumber as expected from the *Middle* panel of Figure 6. The overall spectrum mimics a broken power law with a spectral break near $k \simeq 0.5\Omega_p/v_A$ (for the assumed plasma parameters). The anisotropic tensor (dashed) gives a much sharper cutoff at $k \sim 1/\rho_p$ in agreement with the results of Howes et al. (2007), where ρ_p is the gyroradius of the thermal protons. Note that $v_A \approx v_{th,p}$ for the assumed plasma parameters. *Middle*: Same as the *Left* but plotted as a function of the frequency. Both spectra cut off at Ω_α though the cutoff of the anisotropic model is sharper. The isotropic model has a broader dissipation range with the overall spectrum mimics a broken power-law with a sharp high frequency cutoff. *Right*: Same as the *Middle* panel but with the Doppler shift due to the relative motion between the solar wind and the spacecraft included. The angle between the magnetic field and solar wind velocity $\theta_{BV} = 38^\circ$ and the solar wind speed $V_{SW} = 517\text{km/s}$. As in the *Left* panel, the spectrum of the isotropic diffusion tensor can be fitted with a broken power law (dotted) with the break frequency $\nu_{bf} = 0.2\text{Hz}$ and the lower and higher frequency spectral indexes $\gamma_1 = -1.7$ and $\gamma_2 = -3.1$, respectively.

models. The spectrum of the isotropic diffusion model is also slightly harder and higher than that of the anisotropic model in the “inertial” range, which is in agreement with our study of the Alfvén turbulence in § 3.

In summary, the above results demonstrate the possibility of a rich variety of spectra for turbulence determined primarily by the plasma parameters; the density n , temperature T , magnetic field B , source size L , and the injected energy flux F_0 and wavenumber $k_0 \sim L^{-1}$ (Smith et al. 2006; Markovskii et al. 2008). These parameters can be derived from MHD simulations, which, in combination with the present diffusion model, can be used to study the free energy dissipation processes in magnetized plasmas quantitatively. The uncertain part of this procedure is the choice of the diffusion tensor. As discussed above we have constructed

tensors that produce many features of turbulence spectra obtained with simulations based on more basic physics. Such simulations are too cumbersome or limited to be useful for comparison with observations of astrophysical sources. But they are important in guiding us to derive the appropriate form of the diffusion tensor that lies at the core of our approach. For a given diffusion tensor, the above discussion demonstrates that one can readily (that means no need of supercomputing power) produce spectra for turbulence, for varied background plasma conditions, which can then be used to determine the heating of the background plasma and acceleration of particles and the resultant radiations. The validity of the chosen diffusion tensor form can be established by comparing the model predictions with existing observations or some simulations (Howes et al. 2008; Gary, Saito, & Li 2008). In the next section we compare the predictions of our models with the observed spectra of magnetic fluctuations in the solar wind.

6. Application to the Solar Wind Turbulence

To apply the model to observations of the solar wind turbulence, one must take into account the Doppler shift due to the relative motion of the spacecraft with respect to the solar wind (Leamon et al. 1999). The observed frequency spectrum $P(\nu)$ is related to the turbulence spectrum as:

$$P(\nu) = \int \mathcal{W}(\mathbf{k}) \delta \left\{ \frac{1}{2\pi} [\mathbf{k} \cdot \mathbf{V}_{SW} + \omega(\mathbf{k})] - \nu \right\} d\mathbf{k} \quad (19)$$

where ν is the spacecraft-frame frequency and δ is the Dirac- δ function. The right panel of Figure 7 shows the $P(\nu)$ for the angle between the magnetic field and solar wind velocity $\theta_{BV} = 38^\circ$ and the solar wind speed $V_{SW} = 517$ km/s. The rest of the model parameters are the same as the middle panel, which would be the observed spectrum for $V_{SW} = 0$ km/s. [The spectrum with respect to the wavenumber k in the left panel can be obtained by replacing the argument of the δ function with $(k - k')$, where k' is the variable of the integration.]

All these spectra can be fitted with broken power-laws with steeper high end declines. To understand this result, we may make the approximation: $\mathcal{W}(\mathbf{k}) \propto k^{-11/3} \Theta[k_c(\theta) - k]$. Then the spectrum on the left panel of Figure 7 is given by $P(k) \propto k^{-5/3} \cos \theta_c(k)$, where $\theta_c(k)$ is the cutoff propagation angle in the dissipation range and is given by the inverse of the function $k_c(\theta)$ shown in Figure 5, which increases monotonically with θ , except for a small range near $\theta = 0$. Clearly, $P(k)$ in the dissipation range is determined by $k_c(\theta)$. Since $k_c(\theta)$ covers more than one order of magnitude, the same is the dissipation range of $P(k)$. The spectrum in the middle panel ($V_{SW} = 0$) is obtained by changing the variable from k to

frequency according to the dispersion relation $\omega(\mathbf{k})$. In the MHD regime $\omega(\mathbf{k}) = v_A k_{\parallel}$, then we have $P(\nu) \propto \nu^{-5/3} \cos^{8/3} \theta_c(k)$. Beyond the MHD regime $\omega(\mathbf{k})$ flattens and approaches Ω_α as $k \rightarrow \infty$. As a result $P(\nu)$ cuts off at $\Omega_\alpha/2\pi$. For the spectrum in the right panel we must carry out the integration in equation (19). For solar wind conditions in general, and for the observations we compare with below in particular, the Alfvén velocity ($v_A = 36.8$ km/s) is more than one order of magnitude lower than solar wind velocity ($V_{SW} = 517$ km/s). One may then ignore the $\omega(\mathbf{k})$ term in the argument of the δ -function in the above integration. Then for an isotropic power-law turbulence spectrum, the shape of $P(\nu)$ will be identical to $P(k)$ in the inertial range. In general, $P(\nu) \propto \nu^{-5/3} \int_0^{\cos \theta_c(k)} \cos^{5/3}(\theta_{BV} - \theta) d \cos \theta$, where $k = 2\pi\nu/V_{SW} \cos(\theta_{BV} - \theta_c)$. The dissipation range of $P(\nu)$ starts at $\nu_d \sim V_{SW} k_c(0^\circ) \cos \theta_{BV}/2\pi \sim 0.1$ Hz for the parameters in Figure 7, where we have assumed that $k_c(\theta)$ increases monotonically with $\sin \theta$.

The break frequency of the broken power law fit will be at a higher frequency; $\nu_{bf} \sim V_{SW} k_c(\theta_{BV})/2\pi$. By fitting $P(\nu)$ with a broken power law model down to the power spectral level of 2×10^{-4} nT²/Hz, we obtain the dotted line in the right panel of Figure 7 with $\nu_{bf} = 0.2$ Hz, and the lower and higher frequency spectral indexes $\gamma_1 = -1.7$ and $\gamma_2 = -3.1$, respectively. (For clarity the dotted line is shifted upward by a factor 2.) This broken power law spectrum is very similar to those observed in the solar wind (Leamon et al. 1998, 1999).

6.1. Fit to Observed Spectra

As an example, we fit the observed solar wind turbulence spectrum at 2200UT, January 11, 1997 at 1 AU from the Sun (Leamon et al. 1999), as shown by the solid line in Figure 8. The observation shows that $\theta_{BV} = 38^\circ$, $V_{SW} = 517$ km/s, $B = 63\mu\text{G}$ [$\Omega_p = 0.096(2\pi)\text{Hz}$], and $\beta_p = 0.48$. The Alfvén velocity (or the plasma density or temperature) is not given by the authors. By adjusting v_A and the energy flux F_0 carried by the turbulence, we obtain the best fit to the observed spectrum *for the locally isotropic diffusion tensor model* as shown by the dashed line in the Figure 8. Leamon et. al. (1999) fit the observation with a broken power law model with indexes $\gamma_l = -1.67$, $\gamma_h = -2.91$, and a break frequency $\nu_b = 0.235\text{Hz}$. Our simulated spectrum, when fitted by a broken power law model down to $2 \times 10^{-4}\text{nT}^2/\text{Hz}$, gives $\gamma_1 = -1.67$, $\gamma_2 = -2.97$, and $\nu_{bf} = 0.200\text{Hz}$. F_0 is determined by the turbulence spectrum in the inertial range. With v_A as the only free model parameter, the model reproduces not only the observed break frequency ν_{bf} , but also the power-law index in the dissipation range. This is the most appealing success of the model. Our model fit gives $v_A = 34$ km/s, $n_e = 14$ cm⁻³ for $k_B T_e = 3.35$ eV, which can be compared with

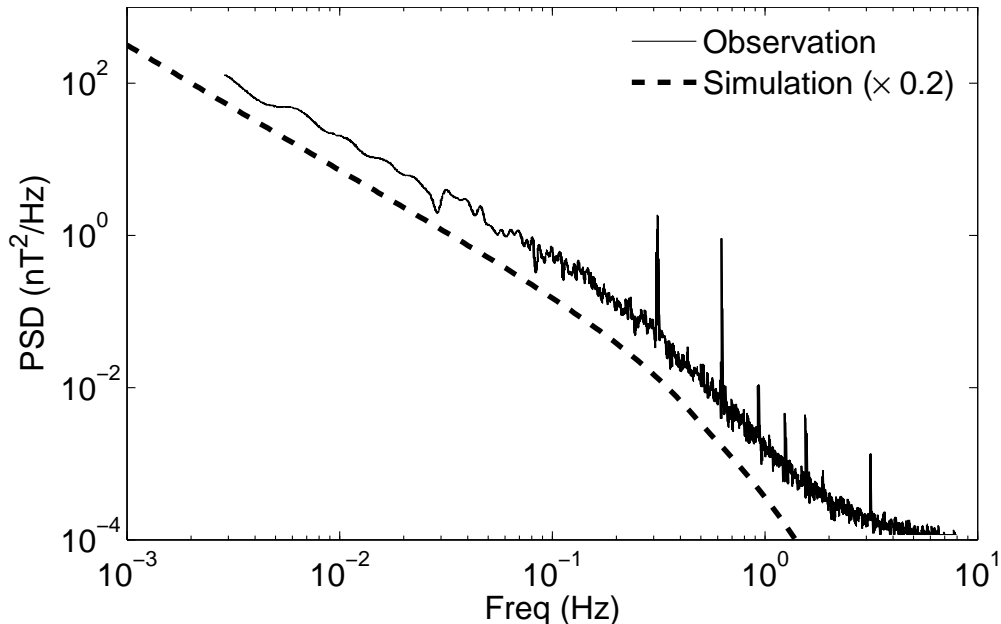


Fig. 8.— Observed interplanetary turbulence power spectrum (solid line; extracted from Figure 1 of Leamon et. al. 1999) compared with our model spectrum (dashed line; scaled downward by a factor of 5 for clarity) based on the locally isotropic diffusion tensor and the model parameters $B = 6.3\text{nT}$, $\beta_p = 0.48$, $\theta_{BV} = 38^\circ$, $V_{SW} = 517\text{km/s}$ given by the observations. The Alfvén velocity is not well determined. Our best fit model has an Alfvén velocity of 34 km/s. The observed spectral flattening at high frequencies is related to a spacecraft noise. As evident this model with essentially only one free parameter provides an excellent fit to the observed spectrum. We note that this model is incompatible with the known properties of Alfvén turbulence, such as those studied by Goldreich & Sridhar (1995).

observations.¹²

We also find that the model based on the anisotropic diffusion tensor cannot fit the observed spectrum very well. This is primarily due to the dominance of the perpendicular component and the much sharper cutoff in the dissipation range as shown by the dashed lines in Figure 7 for the angle averaged spectra. We also consider the Kolmogorov phenomenology

¹²The cascading constant C in equation (4) should be considered as another parameter. There is also an uncertainty in the definition of the eddy speed. For this simulation, we set $C = 1$. A complete measurement of the properties of solar wind plasmas and the turbulence carried by them can be used to determine C and test the model (Yeung & Zhou 1997).

with the isotropic cascade rate $\tau_{\text{cas}}^{-1} \propto k^{2/3}$ in the inertial range. The damping rate is very sensitive to k but has relatively weak dependence on θ (Fig. 5). So k_c , which is identical to the contour of the damping rate, has a weaker dependence on θ than the isotropic diffusion model studied above. As a result, the angle averaged spectrum has a sharper cutoff at high frequencies similar to the anisotropic diffusion model.

Considering the kinetic effects on the wave cascade and damping in the perpendicular direction along the line defined by the critical balance proposed by Goldreich & Sridhar (1995), Howes et al. (2007, 2008a) argue that a 1D diffusion model can also produce a broken-power like spectrum with a cutoff at small spatial scales. In this model, the kinetic Alfvén wave (KAW) has a steeper spectrum than the Alfvén waves. However, to have significant change in the spectral shape between the Alfvén and KAW waves, the electron temperature needs to be much higher than the proton temperature to make the kinetic effects significant. This is quite different from our model, where a broken-power like spectrum is produced by the anisotropic damping and the inhomogeneous cascade in the wavevector space. The broken power-law spectrum they produced is with respect to the perpendicular component of the wavevector. To compare with solar wind observations, one needs to take into account the Doppler effects. The KAW starts at $k_{\perp}\rho_p \approx 1$. The corresponding Doppler-shifted frequency

$$\nu \approx \mathbf{k} \cdot \mathbf{V}_{SW}/2\pi \geq k_{\perp}\rho_p \frac{V_{SW,\perp}}{v_A\beta_p^{1/2}} \frac{\Omega_p}{2\pi}. \quad (20)$$

For typical solar wind conditions with $\beta_p \leq 1$ and $V_{SW} \sim 10v_A$, this frequency is more than 10 times higher than the proton gyro-frequency, which disagrees with the observed fact that the break frequency is usually slightly higher than $\Omega_p/2\pi$ (Leamon et al. 1998, 1999; Bale et al. 2005). With the 1D model, Stawicki et al. (2001) argues that the broken power-law spectrum of the solar wind turbulence may be attributed to the dispersive effects alone as the turbulence cascades from the Alfvén wave domain to the whistler wave regime. However, the diffusion coefficient must be prescribed properly to reproduce the observed spectrum.

From the above discussion we conclude that the model based on the locally isotropic diffusion tensor provides the most natural explanation of the observed solar wind turbulence spectrum. All other models need fine-tuning of the model parameters or relevant physical processes to give acceptable fits to the observed turbulence spectrum.

6.2. Spectral Features and Model Parameters

The previous section shows the success of the model in accounting for a specific observation interval. To understand the nature of the observed broken power spectrum, statistical

studies of a large sample of events are necessary. Some of these studies (Leamon et al. 1998; Smith et al. 2006; Markovskii et al. 2008; Hamilton et al. 2008) have uncovered the nonlinear nature of the dominant dynamics and have shown that several factors may affect the spectral shape in the dissipation range. For a qualitative comparison with these observations, in this section we explore the dependence of the spectral features on the model parameters.

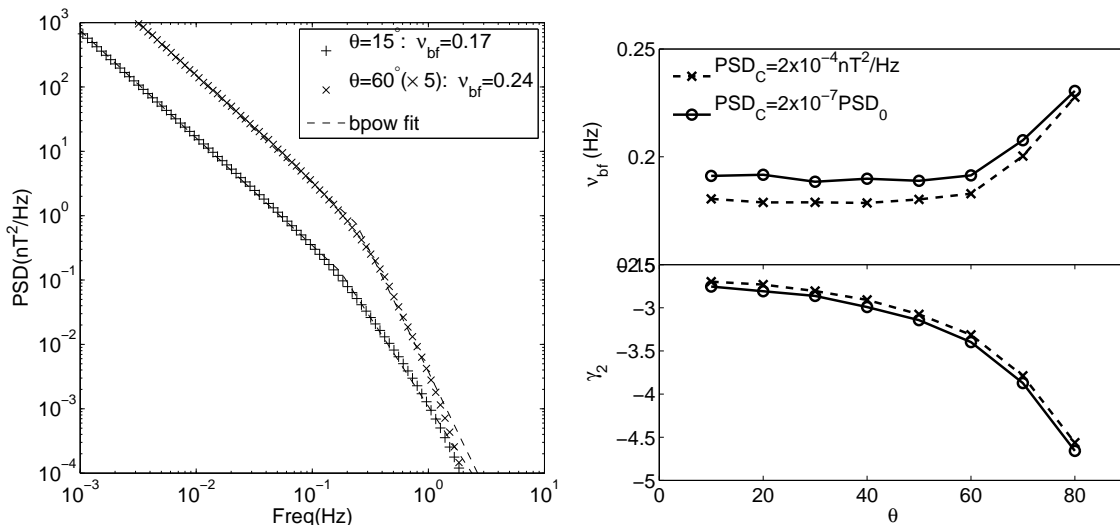


Fig. 9.— Dependence of the angle averaged spectrum on θ the angle between the magnetic field and solar wind velocity (the same as the θ_{BV} in the text). *Left*: Two sample spectra with $M_A = 1.23$, $\beta_p = 0.41$, and two values of θ_{BV} as indicated in the legend. The other parameters are the same as in the right panel of Figure 7. Broken power law fits to these spectra down to $2 \times 10^{-4} \text{ nT}^2 \text{ Hz}^{-1}$ give a break frequency $\nu_{bf} = 0.17$ Hz for $\theta_{BV} = 15^\circ$ and $\nu_{bf} = 0.24$ Hz for $\theta_{BV} = 60^\circ$. *Right*: Dependence of ν_{bf} and γ_2 on θ_{BV} . Two lower limits of the power spectrum are considered while fitting the spectrum with broken power laws. The cross signs are obtained by fitting the model spectrum down to a turbulence power level of $2 \times 10^{-4} \text{ nT}^2 \text{ Hz}^{-1}$, and the circle signs correspond to a low limit of $2 \times 10^{-7} P(\nu = 10^{-3} \text{ Hz})$.

As indicated above, most observed spectra can be fitted with three parameters; γ_1 that is always nearly equal to $-5/3$, γ_2 , and the break frequency ν_{bf} . We have explored the dependence of the latter two on the observable parameters using the locally isotropic diffusion tensor scheme. Figures 9, 10, and 11 show the dependence of the spectrum on θ_{BV} , plasma beta β_p , and Mach number M_A , respectively. The other parameters of the plasma and the injected turbulence are the same as that in the right panel of Figure 7 unless specified otherwise. To describe the spectrum quantitatively, we fit the numerically calculated spectra

to a broken power-law model down to a turbulence power level of $2 \times 10^{-4} \text{ nT}^2\text{Hz}^{-1}$ and $2 \times 10^{-7} P(\nu = 10^{-3}\text{Hz})$. The former is appropriate to compare with observations made by instruments with a given sensitivity to the magnetic field turbulence power. The latter is appropriate for observations with a given dynamical range in the turbulence power spectrum. In general, ν_{bf} and γ_2 are very similar for these two fits, and as stated above, γ_1 is always very close to $-5/3$ for the parameter space explored. The most distinct feature of these results is the correlation between the two observables ν_{bf} and γ_2 (Fig. 12). A higher ν_{bf} always comes along a softer dissipation range spectrum. The correlation caused by variations in β_p and M_A is related to the kinetic effects of the waves beyond the MHD regime. The damping rate is very sensitive to β_p , as can be seen from the right panel of Figure 7. The change in M_A leads to different dissipation scales, where the kinetic effects are different. The resultant correlation between ν_{bf} and γ_2 is mostly caused by the fact that the cascade rate becomes more isotropic near Ω_α (the left panel of Fig. 5). With the decrease of the dissipation scales caused by either higher values of M_A or lower values of β_p , the dissipation range covers a narrower spatial extension, giving rise to a softer dissipation range spectrum. The dependence on θ_{BV} , on the other hand, is mostly due to the Doppler shift. Since $\nu_{bf} \sim V_{SW}k_c(\theta_{BV})/2\pi$, ν_{bf} increases with $\sin\theta_{BV}$, and the spectral range beyond ν_{bf} becomes narrower leading to lower values of γ_2 . These explain the nearly identical correlation between γ_2 and ν_{bf} caused by variations in β_p and M_A while a quite distinct correlation due to changes in θ_{BV} , as shown in Figure 12.

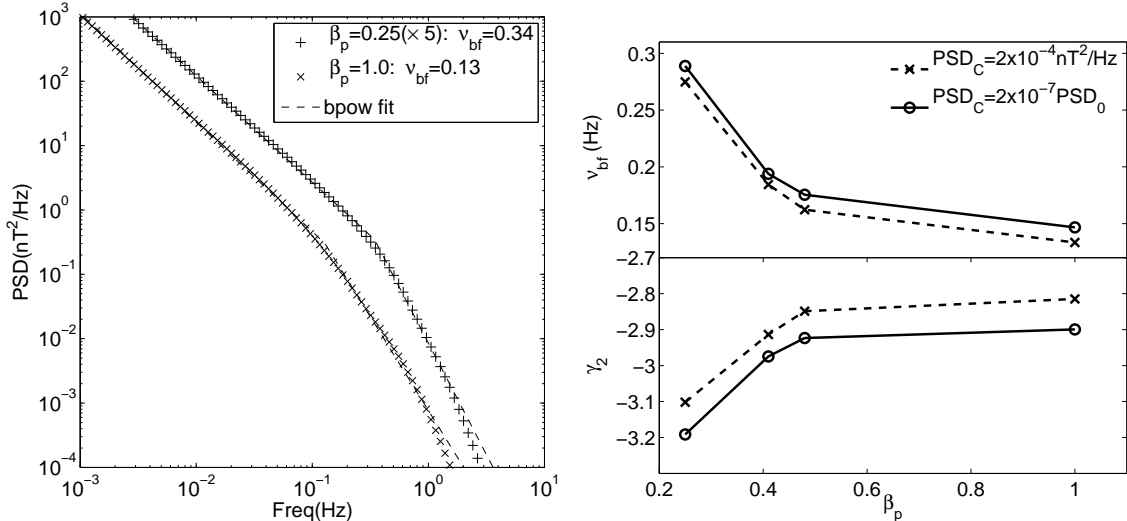


Fig. 10.— Same as Figure 9 but for the dependence on β_p . Here $M_A = 1.23$ and $\theta_{BV} = 38^\circ$.

However, the dependence of the spectrum on θ_{BV} in our model is much weaker than

any quasi-2D turbulence models with the energy cascading only in the perpendicular direction (Howes et al. 2007, 2008a). If most of the wave energy resides in the perpendicular direction, as suggested by the critically balanced cascade proposed by Goldreich & Shridhar (1995), the k_c contour will be highly prolonged in the perpendicular direction and θ_{BV} will strongly affect the break frequency. The observations by Leamon et al (1998, Fig. 6) and by Osman & Horbury (2007) appear to favor the isotropic diffusion model used here (Hamilton et al. 2008). The dependence of the spectrum on the solar wind speed is relatively simple. Obviously, a faster solar wind gives a higher break frequency. Clearly, more observations and/or systematic analyses of existing data are required to test the validity of these models.

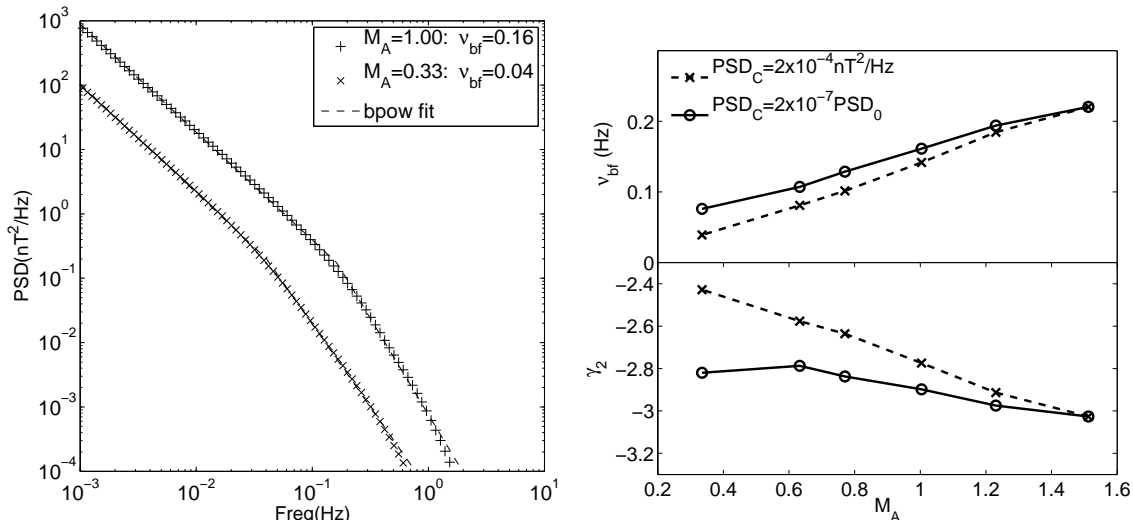


Fig. 11.— Same as Figure 9 but for the dependence on M_A . Here $\beta_p = 0.41$ and $\theta_{BV} = 38^\circ$.

In fact there are already some preliminary results showing some weak correlations (with lots of scatters) between the spectral features and other parameters. For example, the Figure 3 of Leamon et al. (1998) shows a correlation between the break frequency and the proton cyclotron frequency. For a given thermal pressure, higher values of proton cyclotron frequency imply lower values of β_p , and as shown in Figure 10, we expect higher break frequencies as observed. Their Figure 6 shows two events with distinct values of θ_{BV} but similar values for the rest of the parameters. This observation suggests the dissipation range spectrum is harder for higher values of θ_{BV} in contradiction with our Figure 9. However, their spectrum with a higher value of θ_{BV} shows prominent noise at high frequencies so that the spectral break is obscured. Their Figure 2 suggests that the dissipation range spectrum is softer for higher values of proton temperature T_p , which implies higher values of β_p for a

given Alfvén speed. While we expect the opposite, we notice that the higher values of β_p likely result from higher values of M_A , as indicated by the convergence of their inertial range spectral index with the increase of T_p ,¹³ and simultaneous increases of M_A and β_p can make the dissipation range spectrum change in either direction. Indeed, Smith et al. (2006) found that the dissipation range spectrum becomes softer with the increase of the energy cascade rate in the inertial range. According to our model, the energy cascade rate is determined by M_A and k_0 . Thus this observation has the same trend as the dependence of γ_2 on M_A shown in Figure 11.

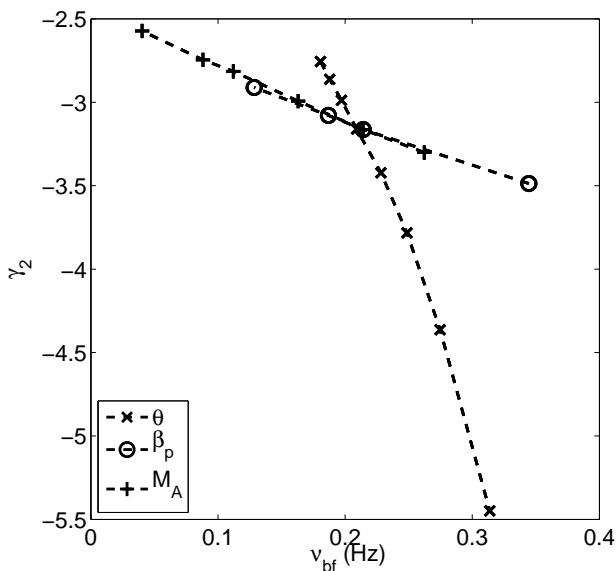


Fig. 12.— The correlation between ν_{bf} and γ_2 caused by variations in θ (crosses), β_p (circles), and M_A (pluses). The model parameters are the same as those in the right panel of Figure 7.

Leamon et al. (1999, Fig. 2) showed a weak correlation between k_{diss} (the same as our k_c) and the inverse of the proton gyro-radius R_L (the same as our ρ_p). For damping dominated by cyclotron resonances, $k_{\text{diss}}C_S \simeq \Omega_p$, where C_S is the sound speed. Therefore $\nu_{bf} \propto k_{\text{diss}} \propto \Omega_p/v_A \sqrt{\beta_p}$, which is similar to the trend we find in Figure 10. In general, higher values of R_L imply higher values of β_p and longer dissipation scales. Smith et al. (2001) studied a solar wind interval with very high Alfvén speeds and found that the cutoff frequency ν_{bf} decreases with the increase of v_A . They concluded from this that the dissipation is related

¹³The inertial range spectrum can be fully developed in shorter periods for turbulence with higher values of M_A .

to the ion inertial length v_A/Ω_p , instead of R_L . We note that the turbulence intensity was very low during this interval, which implies low values of ν_{bf} according to our Figure 11. More recently, Markovskii et al. (2008) correlated the break frequency ν_{bf} with several parameters and found some weak correlations. For example, their Figures 4 and 7 also show a decline of break frequency with the plasma beta; $\nu_{bf} \propto \beta_p^{-x}$ with $x \sim 0.24$, in agreement with our Figure 10. On the other hand, their Figure 6 can be interpreted as $\nu_{bf} \propto 1/M_A$, which has the opposite trend to what we find in Figure 11.

We only have qualitative comparisons of these observations with our model here since the turbulence spectrum depends on several parameters, M_A , θ_{BV} , V_{SW} , β_p , k_0 etc. Simple correlations between γ_2 , ν_{bf} and any one of these quantities are not expected because variations caused by the other parameters may produce significant scatters in the observed data. Clearly, one has to apply the model directly to the observed data to assess its merit. For some events with detailed observations over a large dynamical range, one may use the large scale turbulence spectrum as input to test the diffusion approximation we have promoted here. In some cases, the time dependence of the turbulence spectral evolution may also need to be considered, especially in cases with strong anisotropy observed at large scales (Matthaeus et al. 1990; Dasso et al. 2005; Osman & Horbury 2007).

Our current model only consider the Alfvén-Cyclotron branch. To explain the observed spectrum above 10 Hz (Denskat et al. 1983), one may have to include the fast wave mode branch, which extends up to the electron cyclotron frequency (Appendix A). Another important observational feature is the high magnetic helicity and the enhancement of the parallel magnetic field fluctuations in the dissipation range as compared with the inertial range (Leamon et al. 1998, 1999; Hamilton et al. 2008). Considering the polarized characteristics of the waves, our diffusion model can readily produce results that can be compared with these observations.

7. Conclusion

The free energy dissipation in collisionless astrophysical plasmas plays crucial roles in our understanding of all kinds of nonthermal phenomena. Given the large amount of energy inferred from observations of these nonthermal astrophysical sources, the free energy must come from large scale structures, while the plasma heating and particle acceleration usually start on microscopic scales. An energy cascade from large to small scales is therefore necessary. Strong turbulence is expected to mediate this energy dissipation in many astrophysical sources, and high energy particles, which are responsible for most of the observed emission, compete with the low energy background particles to share this energy. There are currently

no theories, which can address the energy partition between low and high energy particles under different astrophysical conditions. And the major challenges reside in the not-well-known nature of turbulence in magnetized collisionless plasmas. Although there is already much research both numerical and theoretical on turbulence, none of them gives quantitative predictions on the nature of the high energy particles produced in this free energy dissipation process. In this paper we have proposed the treatment of turbulence cascade using the diffusion approximation in the 2D wavevector space, with the aim of treating the free energy dissipation mediated by magnetized turbulence self-consistently. To simplify the problem, we assume that the low energy particles reach a thermal equilibrium. One therefore can study the turbulence cascade and damping by solving the kinetic equation for the turbulence power spectrum numerically.

The diffusion tensor is the central part of the model. Based on previous analytic and numerical results, we have tested two forms for the diffusion tensor; one locally isotropic and one anisotropic. We compare the cascade process of Alfvén-cyclotron turbulence for these two models. As expected the resultant spectra tend to be more anisotropic for the anisotropic tensor but in both cases the energy flux is predominately in the direction perpendicular to the large scale magnetic field, which is qualitatively (but not quantitatively) similar to the Goldreich & Sridhar (1994, 1995) critical balance cascade. The isotropic model for Alfvén turbulence has a critical balance of $k_{\parallel} \propto k^{3/4}$ determined by the diffusion tensor chosen. The critical balance of the anisotropic tensor is almost identical to the Goldreich & Sridhar (1995) relation.

As cascade proceeds to smaller scales ($k \rightarrow \Omega_p/v_A$), the dispersion relation begins to deviate from the simple form valid in the MHD regime. We have included this effect (using two reasonable forms for τ_W) and shown that the turbulence spectrum steepens when we reach this regime. We also show that the inclusion of thermal damping (based on the hot plasma dispersion relation) induces cutoffs in the spectrum as the waves and turbulence dissipate and heat the plasma or accelerate particles. These cutoffs are also very anisotropic and occur at different wavenumbers for different angles of propagation. As a result of these anisotropies, the angle averaged spectra resemble a broken power law both in the wavenumber or frequency domain. We emphasize that this broken power law spectrum requires anisotropy in the cascade as well as damping.

We compare these spectra with those observed in the solar wind by Leamon et. al. (1999) and find a good fit to the observations with the isotropic diffusion tensor model with essentially one free parameter, i.e., the gas density, which is readily observable with the current instruments in space. Based on this model, we also make predictions on the variation of the break frequency and spectral “index” in the dissipation range with the angle between

the magnetic field and solar wind velocity, Alfvén Mach number, and plasma beta. Some of these results appear to be in agreement with the weak correlations found recently with the statistical analyses of a large sample of events (Markovskii et al. 2008).

Our model is distinct from existing 1D models (Stawicki et al. 2001; Galtier 2006; Howes et al. 2008a) for the observed broken power law spectrum of solar wind turbulence. Stawicki et al. (2001) essentially used the observed spectrum to infer the required diffusion coefficient for the wave power spectrum. The weak turbulence theory of Galtier (2006) retains only cascade in the perpendicular direction. In Howes et al. (2008a) model, a critical balance is assumed, which essentially leads to a 1D problem. Due to difficulties in producing a broken power law spectrum with the dissipation processes, all these models invoke some kinetic effects of the wave dispersion on the turbulence energy cascade. Although for the particular event observed by Bale et al. (2005), it appears that kinetic effects play dominant roles. The varieties of the observed high frequency solar wind turbulence spectrum suggest that dissipation processes should play an important role since the kinetic effect induced spectral break does not vary significantly for different observation intervals. In Howes et al. (2008a) model, both kinetic and dissipation processes are considered to produce a varieties of solar wind turbulence spectrum. Cranmer & van Ballegooijen (2003) were the first to study a truly 2D model. However, the model was constructed with a much complicated approach to recover the critical balance proposed by Goldreich & Sridhar (1995) and it hasn't been applied to the solar wind turbulence directly. With the diffusion approximation, our model is simplified significantly. Although the diffusion approximation may not be well justified, especially for weak turbulence, observations can be used to guide the construct of the diffusion tensor and the wave kinetic equations. Direct and more systematic applications of these models to the observed solar wind spectra will be able to test them.

We thank Christopher L. Fryer, Hui Li, and Alex Lazarian for helpful discussions and the referee for a critical review. The research at Stanford is partially supported by NSF grant ATM-0312344, NASA grants NAG5-12111, NAG5 11918-1. This work at the Los Alamos National Laboratory was carried out under the auspices of the National Nuclear Security Administration of the U.S. Department of Energy under Contract No. DE-AC52-06NA25396, and received partial support from the EU's Solaire Research Training Network at the University of Glasgow (MTRN-CT-2006-035484).

APPENDICES

A. Cold Plasma Dispersion Surface

The stochastic particle acceleration theory is built on wave-particle resonant interactions, and the plasma turbulence cascade also highly depends on the wave-wave resonances. To investigate these resonant interactions, and the acceleration and cascade processes, an exact form of the plasma dispersion relation is required. However, a complete treatment of the coupled oscillations of particles and fields is too complicated to provide even a stable numerical solution that can be integrated into the numerical study of wave-particle or wave-wave resonant interactions. By introducing a cold plasma approximation, Stix (1962) solved the complete dispersion relation analytically. In this section we discuss the solution of the cold plasma dispersion relation and the procedure of isolating individual wave mode for the turbulence cascade and particle acceleration study.

Although the solution of cold plasma dispersion relation is segmented and has poles at particle cyclotron frequencies (Swanson 1989), each physical mode of dispersion surface is both continuous and smooth almost everywhere. Thereafter, one can isolate each continuous mode with segmented functions that gives $k(\omega, \theta)$ relationship by one-to-one mapping. In this subsection, we discuss the dispersion relation and the range of each wave mode specifically with the notation given by Swanson (1989).

Alfvén-He Cyclotron branch,

$$k = \omega \sqrt{\frac{B - F}{2A}} \quad \omega \in [0, \Omega_\alpha) \quad (\text{A1})$$

R and L term reach their first pole (Ω_α) and $\lim_{\omega \rightarrow \Omega_\alpha^-} k = \infty$. This cutoff frequency is the end of the Alfvén branch.

Fast-Proton Cyclotron branch,

$$k = \begin{cases} \omega \sqrt{\frac{B + F}{2A}} & \omega \in [0, \Omega_\alpha^-] \\ \omega \sqrt{\frac{B - F}{2A}} & \omega \in [\Omega_\alpha^+, \Omega_p) \end{cases}$$

Similarly, the fast branch cuts off at Ω_p with $k_{\parallel} \rightarrow \infty$. Although Ω_α is a pole for R and L , $\lim_{\omega \rightarrow \Omega_\alpha^-} \frac{B + F}{2A} = \lim_{\omega \rightarrow \Omega_\alpha^+} \frac{B - F}{2A} \neq \infty$, i.e. the dispersion surface is continuous. The

switch of sign at Ω_α can be easily explained in a simplified case where $\theta = 0$. At $\theta = 0$, $F = 2\sqrt{P^2D^2} = 2 |PD|$ and the wave solution (Swanson 1989) simplifies into

$$k = \omega \left(S \pm \frac{|PD|}{P} \right)^{1/2} = \omega (S \pm \text{sign}(PD)D)^{1/2} \quad (\text{A2})$$

Since $P < 0$ for all $\omega \in [0, 1]$, and D switches sign at Ω_α whereas $(P^2D^2)^{1/2}$ does not, the discontinuity is only introduced by the attempt of writing $k(\omega)$ in an explicit form. As a result, by switching the sign in $\frac{B \pm F}{2A}$ at $D = 0$, we can follow the continuous dispersion surface.

Whistler branch,

$$k = \begin{cases} \omega \sqrt{\frac{B+F}{2A}} & \omega \in [\omega_1, \Omega_p) \\ \omega \sqrt{\frac{B-F}{2A}} & \omega \in (\Omega_p, \omega_e) \end{cases}$$

Due to the strong He cyclotron (left-handed) damping around Ω_α , $\frac{B+F}{2A}$ becomes pure imaginary at $[\Omega_\alpha, \omega_1)$, where ω_1 is the smaller root of equation $R(\omega) = 0$. This ω_1 is the starting point of Whistler branch ($\omega_1 \approx 0.585\Omega_p$ very insensitive to density and field strength). On the other hand, at ω_e we get $P = 0$, the formula reach the pole in parallel direction ($\theta = 0$), and the Whistler branch cuts off at the electron Langmuir oscillation.

In the parallel direction, the fast branch starts with electron cyclotron branch and turns into proton cyclotron branch; the whistler branch, on the other hand, starts with proton cyclotron branch and turns into electron cyclotron branch (Petrosian & Liu 2004). As shown in Figures 13 and 14, this turning point is also the crossing point of electron cyclotron and proton cyclotron branches. If we assume turbulence can only start at large scales and low frequency, this would be the only point where whistler branch and even higher frequency branches obtain energy from the turbulence cascade. This crossing wavenumber k_c and the efficiency of reverse cascade determine the low wavenumber cutoff on energy spectrum of proton cyclotron branch, k_{\min} , which in turn determines the acceleration efficiency on ions, especially ^3He due to its special charge to mass ratio (see Liu et al. 2006 for a detailed discussion of how k_{\min} affects ^3He spectrum). Thereafter, it is worthwhile to calculate this crossing point. By solving $\frac{B+F}{2A} = \frac{B-F}{2A}$ (i.e. $D = 0$) or

$$\frac{-\Omega_e\omega_e^2}{\omega^2 - \Omega_e^2} + \frac{-\Omega_p\omega_p^2}{\omega^2 - \Omega_p^2} + \frac{-\Omega_\alpha\omega_\alpha^2}{\omega^2 - \Omega_\alpha^2} = 0 \quad (\text{A3})$$

we get $\omega_2 = 0.615\Omega_p$ ¹⁴ and the corresponding wavenumber

$$k_c = \sqrt{460.5\alpha^2 - 10^{-12}\alpha + 0.377\Omega_p}/c \quad (\text{A4})$$

where $\alpha = \omega_e/\Omega_e = \sqrt{4\pi n_e m_e c}/B$ is the only free parameter for the dispersion relation with the cold plasma approximation.

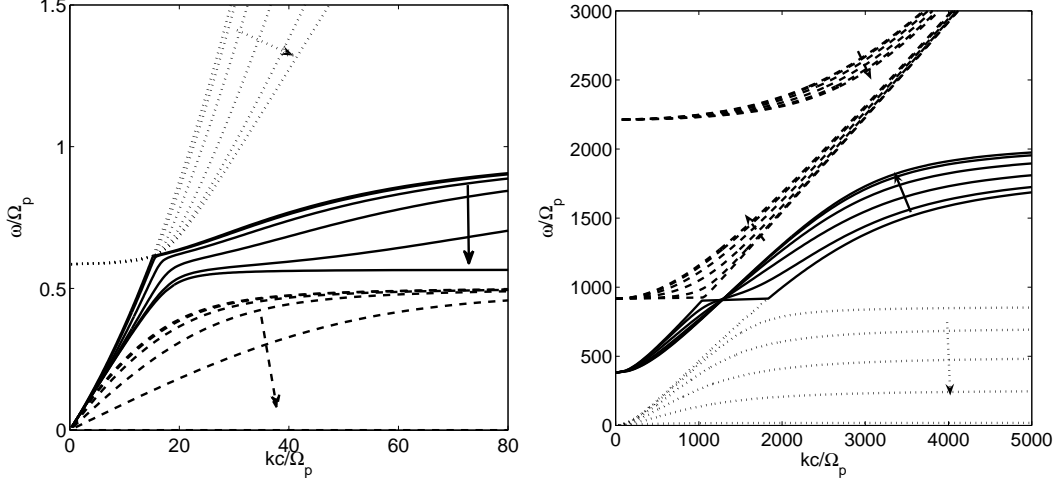


Fig. 13.— The dispersion relation for a cold fully ionized H and He (10% by number) plasma at different angles ($\theta = 0, \pi/10, \pi/5, 3\pi/10, 2\pi/5, \pi/2$ with arrows pointing to the direction of increasing angle). In this example, the only free parameter $\alpha \equiv \omega_{p,e}/\Omega_e = 0.5$. *Left:* Alfvén (dashed), Fast (solid) and low frequency segment of Whistler branch (dotted). *Right:* High frequency segment of Whistler branch (dotted), Upper Hybrid (solid) and the two EM branches (dashed).

Upper hybrid branch,

$$k = \begin{cases} \omega \sqrt{\frac{B+F}{2A}} & \omega \in [\omega_3, \Omega_e) \\ \omega \sqrt{\frac{B-F}{2A}} & \omega \in (\Omega_e, \omega_4) \end{cases}$$

The upper hybrid branch starts at ω_3 , which is the second root of $R(\omega) = 0$, and it becomes electron cyclotron wave in parallel direction. It extends to higher frequencies in other direction and reaches the resonance frequency ω_4 in perpendicular direction.¹⁵

¹⁴This result depends on the particle mass and relative abundance only, which are approximately constant.

¹⁵In the perpendicular direction $n^2 = \frac{RL}{S}$, so ω_4 is the root of $S = 0$

At even higher frequency, there are two electromagnetic wave (EM) branches. The lower one is,

$$k = \begin{cases} \omega \sqrt{\frac{B-F}{2A}} & \omega \in [\omega_{p,e}, \Omega_e) \\ \omega \sqrt{\frac{B+F}{2A}} & \omega \in (\Omega_e, \infty) \end{cases},$$

and the higher branch is

$$k = \omega \sqrt{\frac{B-F}{2A}} \quad \omega \in [\omega_5, \infty), \quad (\text{A5})$$

where ω_5 is the root of $L = 0$.

With these segmented functions, one can construct an analytical one-to-one $k(\omega, \theta)$ mapping. Thereafter, the explicit dispersion relation $\omega(\mathbf{k})$ can be easily solved numerically. Figure 13 shows the calculated dispersion surface for a typical solar flare conditions. The accuracy and stability of the dispersion relation obtained by solving these equations will facilitate the numerical study on wave particle interaction or turbulence cascading.

B. Damping and Hot Plasma Dispersion Relation

The cold plasma approximation ignores any thermal motion of charged particles, and therefore, limits the resulting dispersion relation to scales larger than the thermal kinetic gyroradius. In the damping phase, there are strong couplings between the charged background particles and turbulent motion, and the background particles are energized. This process is a major mechanism for heating the solar flares and other astrophysical plasmas (Petrosian et al. 2006, Bittner et. al. 2007). On the other hand, the process also significantly damps the plasma turbulence and affects the dispersion relation. To study the dispersion relation as well as damping effects (i.e., the imaginary part of wave frequency $\Im[\omega]$) in the damping range, one needs to study the collective motion of thermal particles. It is easier to use the distribution function $f_j(\mathbf{r}, \mathbf{v}, t)$ to represent the charge and current density,

$$\rho = \sum_j q_j \int d^3v f_j \quad (\text{B1})$$

$$\mathbf{J} = \sum_j q_j \int d^3v \mathbf{v} f_j \quad (\text{B2})$$

where the subscript j stands for species of particle. The particle distribution function f_j satisfies Vlasov equations, which includes,

$$\frac{\partial f_j}{\partial t} + \mathbf{v} \cdot \nabla f_j + \frac{q_j}{m_j} (\mathbf{E} + \mathbf{v} \times \mathbf{B}) \cdot \nabla_v f_j = 0 \quad (\text{B3})$$

and the Maxwell equations.

There are many linear, quasilinear and nonlinear approximations to solve the Vlasov equation set. A detailed introduction to these solutions can be found in Swanson’s *Plasma Waves* (1989). To study turbulence cascading and particle acceleration, we only use an analytical approximation for parallel propagating waves and the numerical nonlinear approximation with the WHAMP (Waves in Homogeneous, Anisotropic, Multicomponent Plasmas by Ronnmark 1982) code for non-parallel propagating waves.

B.1. Damping of Parallel Propagating Waves

The parallel propagating waves are extensively studied in stochastic acceleration theory due to its simplicity and efficiency in accelerating particles. The theory is used to explain the electron and ion spectra and ^3He enrichment from solar flares (Petrosian & Liu 2004; Liu et al. 2004; 2006 on ^3He rich impulsive solar energetic particle events). These studies show that the turbulence energy spectrum and its high wavenumber cutoff due to damping are important factors that determine the accelerated particle spectra and relative abundance. In this subsection, we calculate the damping rate and the cutoff point for parallel propagating waves with the linear approximation.

For parallel and quasi-parallel propagating waves, the Dielectric Tensor can be simplified and provide the dispersion relation for right-handed cyclotron wave (R -wave) and left-handed cyclotron wave (L -wave) (Swanson 1982, p. 158),

$$\frac{k^2}{\omega^2} = 1 + \sum_j \frac{\omega_{pj}^2}{\omega k_z v_j} \left[\left(\frac{1 \pm \epsilon_j}{2} \right) Z(\zeta_{1j}) + \left(\frac{1 \mp \epsilon_j}{2} \right) Z(\zeta_{-1j}) \right] \quad (\text{B4})$$

where $\omega = \omega_r + i\omega_i$ is the complex wave frequency, v_j here is thermal velocity, $\zeta_{nj} = \frac{\omega + n\Omega_j}{kv_j}$ is a shorthand, and

$$Z(\zeta_{nj}) = \frac{1}{\sqrt{\pi}} \int_{-\infty}^{\infty} \frac{e^{-\xi^2} d\xi}{\xi - \zeta} \quad (\text{B5})$$

is the Plasma Dispersion Function that can be approximated with

$$Z(\zeta) = i\sqrt{\pi}e^{-\zeta^2} - \frac{1}{\zeta} \left(1 + \frac{1}{2\zeta^2} + \frac{3}{4\zeta^4} + \dots \right) \quad (\text{B6})$$

Except for the electromagnetic waves, $\Omega_j \gg kv_j$ for all particle species and all possible

wavenumbers.¹⁶ As a result, the imaginary part of $Z(\zeta)$ for parallel propagating wave is small for most frequencies but increase dramatically around particle's gyrofrequency. For example, despite the summation of all species of particles in Equation (B4), the contribution from ions to the R -wave (electron cyclotron wave is the only R -wave for solar flare or solar wind) dispersion relation is far less than that from electrons. Therefore by considering electron cyclotron term only, Swanson (1982) obtained the damping rate for the R -wave with the first order approximation (Equation B6),

$$\frac{\omega_i}{\omega_r} = -\frac{\sqrt{\pi}\omega_{pe}^2}{\omega_r k v_e \left[2 + \frac{\omega_{pe}^2 \Omega_e}{\omega_r (\omega_r - \Omega_e)^2} \right]} \exp \left[-\left(\frac{\omega_r - \Omega_e}{k v_e} \right)^2 \right] \quad (\text{B7})$$

For the L -wave (for solar flare or solar wind, L -wave includes the helium cyclotron and proton cyclotron wave), the contribution from electron cyclotron term can be ignored. However due to their close gyrofrequency, the contributions of proton and helium cyclotron term become comparable. Thereafter, we generalized Swanson's (1982) derivation to include all the particle into the calculation and obtain the damping rate for parallel propagating waves:

$$\frac{\omega_i}{\omega_r} = -\frac{\sum_s \frac{\sqrt{\pi}\omega_{p,s}^2}{\omega_r k v_s} \exp \left[-\left(\frac{\omega_r - \epsilon_s \Omega_s}{k v_s} \right)^2 \right]}{\frac{2k^2}{\omega_r^2} + \sum_s \frac{2\omega_r - \epsilon_s \Omega_s}{\omega_r (\omega_r - \epsilon_s \Omega_s)^2} \omega_{p,s}} \quad (\text{B8})$$

When damping rate overwhelms cascading rate from below, the turbulence energy spectrum cuts off, and the k_{max} is obtained by solving $\tau_{cas}^{-1} = \tau_{damp}^{-1} \equiv 2\omega_i$. Figure 14 illustrates this procedure of finding k_{max} by assuming a Kolmogorov cascading rate (Zhou & Matthaeus 1990). From the figure We can also see that the cyclotron damping rate grows extremely fast (exponential of a square) at particle's cyclotron frequency and thus k_{max} becomes insensitive to the cascading rate. Thereafter, by fitting to the numerical results of k_{max} , we am able to approximate k_{max} for proton and helium cyclotron branch with plasma temperature and α only,

$$\text{PC: } k_{max} = (110\alpha + 20) \left(\frac{T}{10^6 \text{K}} \right)^{-0.15} - 50\alpha + 8 \quad (\text{B9})$$

$$\text{HeC: } k_{max} = (50\alpha + 5) \left(\frac{T}{10^6 \text{K}} \right)^{-0.16} - 10\alpha + 6 \quad (\text{B10})$$

¹⁶Although cold plasma approximation suggests that k diverges at particle's gyrofrequency, the damping rate at these frequencies diverges too, which prevents the dispersion relation extending to a large wavenumber.

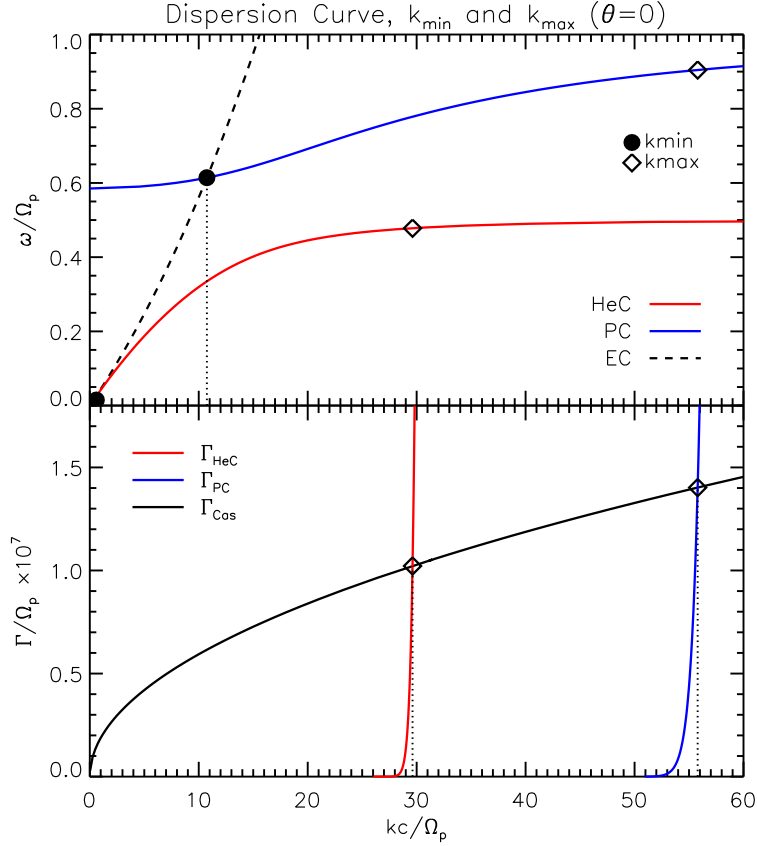


Fig. 14.— Dispersion relation for parallel propagating waves and its high and low wavenumber cutoff, k_{min} and k_{max} . *Upper panel:* The low wavenumber cutoff caused by the topology of dispersion curve i.e., the crossing between EC and PC branch. *Lower panel:* The high wavenumber cutoff generated by cyclotron damping overwhelming cascading. we assume a simple Kolmogorov cascading rate for both PC and HeC branch in this case.

Note that although the formula (B7) and (B8) gives the damping rate ω_i for all \mathbf{k} , the Lauren series approximation of plasma dispersion function (Equation B6) fails at particle's gyrofrequencies ($\lim_{\omega_r \rightarrow \Omega_s} \zeta = 0$, where subscript s stands for different species of particles). At these ranges $\omega_r \simeq \Omega_s$, one can simplify Equation (B4) and show that $\omega_i \ll \omega_r$ (Swanson 1989). Since the accurate number of ω_i becomes unimportant at the range $\omega_i \gtrsim \omega_r$, we simply extrapolate the approximated damping rate with a power law at $\omega_r \simeq \Omega_s$ region for the turbulence cascade and wave-particle interaction studies.

REFERENCES

- André, M. 1985, *J. Plasma Phys.* 33, 1
- Bale, S. D., Kellogg, P. J., Mozer, F. S., Horbury, T. S., & Reme, H. 2005, *Phys. Rev. Lett.*, 94, 215002
- Beresnyak, A., & Lazarian, A. 2008, *ApJ*, 678, 961
- Biskamp, D., Schwarz, E., Zeiler, A., Celani, A., & Drake, J. F. 1999, *Phys. Plasmas*, 6, 751
- Bittner, J. M., Liu, S., Fryer, C. L., & Petrosian, V. 2007, *ApJ*, 661, 863
- Boldyrev, S. 2002, *ApJ*, 569, 841
- Borovsky, J. E., & Funsten, H. O. 2003, *JGR*, 108(A7), 1284, doi:10.1029/2002JA009625, 2003
- Braginskii, S. I. 1965, *RvPP*, 1, 205
- Brown, J. C., & Melrose, D. B. 1977, *SoPh*, 52, 117
- Chandran, B. D. G. 2005, *PRL*, 95, 265004
- Chen, Y., Reeves, G. D., & Friedel, R. H. W. 2007, *Nature*, doi: 10.1038/nphys655
- Cho, J., & Lazarian, A. 2003, *MNRAS*, 345, 325
- Cho, J., & Lazarian, A. 2006, *ApJ*, 638, 811
- Cho, J., Lazarian, A., & Vishniac, E. T. 2002, *ApJ*, 564, 291
- Cho, J., Lazarian, A., & Vishniac, E. T. 2003, *Turbulence and Magnetic Fields in Astrophysics* eds. by E. Falgarone, and T. Passot, *Lecture Notes in Physics*, 614, 56
- Cho, J., & Vishniac, E. T. 2000, *ApJ*, 538, 217
- Cranmer, S. R., & van Ballegoijen, A. A. 2005, *ApJS*, 156, 265
- Cranmer, S. R., & van Ballegoijen, A. A. 2003, *ApJ*, 594, 573
- Dasso, S., Milano, L. J., Matthaeus, W. H., & Smith, C. W. 2005, *ApJ*, 635, L181
- Denskat, K. U., Beinroth, H. J., & Neubauer, F. M. 1983, *J. Geophys.*, 54, 60
- Farmer, A. J., & Goldreich, P. 2004, *ApJ*, 604, 671

- Fletcher, L., & Hudson, H. 2008, *ApJ*, 675, 1645
- Galtier, S. et al., 2000, *J. Plasma Phys.* 63, 447
- Galtier, S. 2006, *J. Plasma Phys.* 72, 721
- Gary, S. P., & Borovsky, E. 2004, *JGR*, 109, A06105
- Gary, S. P., Saito, S., & Li, H. 2008, *Geophys. Res. Lett.*, 35, L02104, doi:10.1029/2007GL032327
- Ginzburg, V. L. 1961, *Propagation of Electromagnetic Waves in Plasma* (New York: Gordon & Breach)
- Ginzburg, V. L., & Syrovatskii, S. I. 1969, *The Origin of Cosmic Rays* (New York: Gordon & Breach)
- Goldreich, P., & Sridhar, S. 1995, *ApJ*, 438, 763
- Hamilton, K., Smith, C. W., Vasquez, B. J., & Leamon, R. J. 2008, *JGR*, 113, A01106
- Howes, G. G. et al. 2007, astro-ph/0707.3149, astro-ph/0707.3147
- Howes, G. G. et al. 2008, *PRL*, 100, 065004, doi: 10.1103/PhysRevLett.100.065004
- Howes, G. G. et al. 2008a, *JGR*, 113, A05103, doi: 10.1029/2007JA012665
- Iroshnikov, P. S. 1963, *AZh*, 40, 742
- Kolmogorov, A. N. 1941, *Dokl. Akad. Nauk SSSR*, 30, 301
- Kraichnan, R. H. 1965, *Phys. Fluids*, 8, 1385
- Krucker, S., Hurford, G. J., MacKinnon, A. L., Shih, A. Y., & Lin, R. P. 2008a, *ApJ*, 678, L63
- Krucker, S., et al. 2008b, *AA Rev*, 16, 155 DOI 10.1007/s00159-008-0014-9
- Lazarian, A., & Beresnyak, A. 2006, *ApJ*, 373, 1195
- Leamon, R. J., Matthaeus, W. H., Smith, C. W., Zank, G. P., Mullan, D. J., & Oughton, S. 1998, *JGR*, 103, 4775
- Leamon, R. J., Smith, C. W., Ness, N. F., Matthaeus, W. H., & Wong, H. K. 1998, *JGR*, 103, 4775

- Leamon, R. J., Smith, C. W., Ness, N. F., & Wong, H. K. 1999, *JGR*, 104, 22331
- Li, H., Gary, S. P., & Stawicki, O. 2001, *Geophys.Res.Letters*, 28, 1347
- Liu, S., Melia, F., Petrosian, V., & Fatuzzo, M. 2006a, *ApJ*, 647, 1099.
- Liu, S., Petrosian, V., & Mason, G. M. 2004, *ApJ*, 613, L81
- Liu, S., Petrosian, V., & Mason, G. M. 2006, *ApJ*, 636, 462
- Liu, S., Fan, Z. H., Fryer, C. L., Wang, J. M., & Li, H. 2008, *ApJL*, in press, astro-ph/0805.2589
- Liu, W., Liu, S., Jiang, Y., & Petrosian, V. 2006b, *ApJ*, 649, 1124
- Luo, Q., & Melrose, D. 2006, *MNRAS*, 368, 1151
- Markovskii, S. A., Vasquez, B., J., & Smith, C. W. 2008, *ApJ*, 675, 1576
- Markovskii, S. A., Vasquez, B., J., Smith, C. W., & Hollweg, J. V. 2006, *ApJ*, 639, 1177
- Mason, G. M., et al. 2002, *ApJ*, 574, 1039
- Matthaeus, W. M., Ghosh, S., Oughton, S., & Roberts, D. A. 1996, *J. Geophys. Res.*, 101, 7619
- Matthaeus, W. M., Goldstein, M. L., & Roberts, D. A. 1990, *J. Geophys. Res.*, 95, 20673
- Matthaeus, W. M., Oughton, S., Ghosh, S., & Hossian, M. 1998, *Phys. Rev. Lett.*, 81, 2056
- Miller, J. A. 1997, *ApJ*, 491, 939
- Miller, J. A., LaRosa, T. N., & Moore, R. L., 1996, *ApJ*, 461, 445
- Miller, J. A., & Roberts, D. A. 1995, *ApJ*, 452, 912
- Montgomery, D., & Matthaeus, W. H. 1995, *ApJ*, 447, 706
- Montgomery, D., & Turner, L. 1981, *Phys. Fluids* 24(5), 825
- Ng, C. S., & Bhattacharjee, A. 1996, *ApJ*, 465, 845
- Ng, C. S., & Bhattacharjee, A. 1997, *Phys. Plasmas*, 4(3), 605
- Oughton, S., Dmitruk, P., & Matthaeus, W. H. 2006, *Phys. Plasmas* 13, 042306
- Osman, K. T., & Horbury, T. S. 2007, *ApJL*, 654, L103

- Park, B. T., & Petrosian, V. 1995, ApJ, 446, 699.
- Parks, G. K., et al., 2006, Phys. Plasma, 13, 050701
- Petrosian, V., & Liu, S. 2004, ApJ, 610, 550
- Petrosian, V., Yan, H., & Lazarian, A. 2006, ApJ, 644, 603
- Porter, D., Pouquet, A., Sytine, I., & Woodward, P. 1999, Physica, A, 263, 263
- Porter, D. H., Woodward, P. R., & Pouquet, A. 1998, Phys. Fluids, 10, 237
- Reames, D. V., Meyer, J. P., & von Roseninge, T. T. 1994, ApJS, 90, 649
- Rönnmark, J. 1982, Waves in Homogeneous, Anisotropic, Multicomponent Plasmas (Sweden: Kiruna Geophysics Institute)
- Saito, S., & Gary, P. 2007, JGR, 112, A06116
- Shebalin, J. V., Matthaeus, W. H., & Montgomery, D. 1983, J. Plasma Phys. 29, 525
- Smith, C. W., Hamilton, K., Vasquez, B. J., & Leamon, R. J. 2006, ApJ, 645, L85
- Smith, C. W., Mulla, D. J., Ness, N. F., Skoug, R. M., & Steinberg, J. 2001, JGR, 106, A9, 18625
- Stawicki, O., Gary, S. P., & Li, H. 2001, JGR, 106, 8273
- Sridhar, S., & Goldreich, P. 1994, ApJ, 432, 612
- Stix, T. H. 1962, *The Theory of Plasma Waves* (McGraw-Hill Book Company, Inc.)
- Swanson, D. G. 1989, Plasma Waves (Academic Press, Boston)
- Tu, C. -Y., Wang, L. -H., & Marsch, E. 2002, JGR, 107, A10, 1291
- Vestuto, J. G., Ostriker, E. C., & Stone, J. M. 2003, ApJ, 590, 858
- Wu, D., & Yang, L. 2006, A&A, 452, L7
- Xie, H., & Ofman, L. 2004, JGR, 109, A08103
- Yan, H., & Lazarian, A. 2002, Phys.Rev.Letters 89, 281102-1
- Yan, H., Lazarian, A., & Petrosian, V. 2008, astro-ph/0801.3786
- Yeung, P. K., & Zhou, Y. 1997, ICASE Report No. 97-64.

Zakharov, V. E., & Kuznetsov, E. A. 1978, JETP, 48, 458

Zhang, T. X., & Li, B. 2004, Phys. Plasmas, 11, 2172

Zhou, Y., & Matthaeus, W. H. 1990, JGR, 95, 14881